10. Magnetic Properties

Magnetic materials are one of the most prominent classes of functional materials, as introduced in Sect. 1.3. They are mostly inorganic, metallic or ceramic in nature and typically multicomponent when used in applications (e.g. alloys or intermetallic phases). Their structure can be amorphous or crystalline with grain sizes ranging from a few nanometers (as in high-end nanocrystalline soft magnetic materials) to centimeters (as in grain-oriented transformer steels). They are available as powders, cast, sintered or composite materials, ribbons or even thin films and find a huge variety of applications in transformers, motors, generators, medical system sensors, and microelectronic devices.

The aim of this chapter is to give advice as to which methods are most applicable to determine the characteristic magnetic properties of any of the materials mentioned above. Magnetic thin-film structures have recently gained significant scientific and economic importance. Not only can their properties deviate from the respective bulk materials but novel phenomena can also occur, such as giant and tunnel magneto-resistance, which lead to their application in read heads and their likely future application to nonvolatile magnetic solid-state memory (MRAM). Therefore, we have added a section that explains the important peculiarities special to thin films, in which we summarize the most relevant measurement techniques.

Section 10.1 will give a short overview to enable the reader to differentiate between the various manifestations of magnetism, different materials and their related properties. For a deeper understanding, of course, textbooks should be used (see the references given in Sect. 10.2). Section 10.2 covers the standard measurement techniques for soft and hard magnetic materials. The tables at the beginning of Sect. 10.2.1 are a valuable guide to choose the best technique for any given property to be measured. It is anticipated that this chapter will cover the overwhelming needs for a routine characterization of soft and hard magnetic materials in their various forms. Section 10.3 introduces an elegant, novel and extremely fast technique, the so-called pulse field magnetometer, to measure the hysteresis loop of hard magnetic materials and thereby to determine the remanent magnetization, the anisotropy field and coercivity, respectively. This method has been developed only recently and is not yet comprehensively covered in textbooks. It is therefore described in more detail with a critical discussion of possible measurement errors and calibration requirements. Finally, as mentioned above, Sect. 10.4 addresses features peculiar to magnetic thin films and recommends techniques for their magnetic characterization. It comprises an overview of magneto-resistive effects occurring in magnetic thin films or multilayers where the electrical resistivity depends on external magnetic fields. These devices find important applications as read heads in hard-disc drives and as sensors in the automotive and automation industries. The standard measurement to determine the field response (change in resistance within a given field range) is simply a resistivity measurement, as described in Chap. 9, except that it needs to be done in an external magnetic field. These electrical techniques are therefore not covered in this chapter.

In bulk and thin-film ferromagnets properties such as remanent magnetization and coercivity often depend on the time scale used in the measurement (Sects. 10.1.6, 10.3.3). Time-dependent measurements needed, e.g., to predict the stability of the material in applications are not explicitly described in this chapter since, in principle, any sensitive magnetometer can be used for these measurements. In research, sophisticated methods are used to resolve magnetization dynamics on pico- or even femtosecond time scales. A detailed description of these more specialized methods is beyond the scope of this handbook.

10.1 Magnetic Materials

Empirically, materials are classified according to their response to an applied magnetic field, i. e. the magnetization induced by the external field. A more fundamental understanding results from considering the microscopic mechanisms that determine the behavior of materials in the magnetic field.

10.1.1 Diamagnetism, Paramagnetism, and Ferromagnetism

Diamagnetism is a property of all materials. It results from an additional orbital angular momentum of electrons induced in a magnetic field. In analogy to the induction of eddy currents in a conductor it manifests itself as a magnetization oriented in the opposite direction to the external field; by definition this is equivalent to a negative susceptibility (definitions are given below).

Paramagnetism means a positive magnetic susceptibility, i. e. the induced magnetization is along the direction of the external magnetic field. It is observed in materials which contain atoms with nonzero angular momentum, e.g. transition metals. The susceptibility scales with $1/T$ (Curie's law). Paramagnetism is also found in certain metals (e.g. aluminum) as a consequence of the spin of conduction electrons (Pauli spin susceptibility). The related susceptibility is essentially independent of temperature. The paramagnetic susceptibility is generally several orders of magnitude larger than the diamagnetic component; therefore, diamagnetism is not observable in the presence of paramagnetism.

Ferromagnetism describes the fact that certain solid materials exhibit a *spontaneous magnetization*, M_S, even in the absence of an external magnetic field. It is a collective phenomenon resulting from the spontaneous ordering of the atomic magnetic moments due to the *exchange interaction* among the electron spins. It is observed in a few transition metals (e.g. 3d, 4f) where itinerant electrons play the essential role for the exchange coupling mechanism, but also in their oxides, halides etc., where the exchange interaction is mediated by localized electrons of oxygen, sulfur etc. atoms located between neighboring metal atoms (*indirect exchange, superexchange*). Recently ferromagnetism has been observed in semiconductors (e.g. GaAs, TiO_2) doped with a few percent of a transition element like Mn, Fe or Co which provides localized magnetic moments and free charge carriers which mediate the exchange interaction among the localized moments. If ferromagnetic order in these materials can be maintained above room temperature (which is currently not certain) they might become useful for future electronic devices based on the spin of electrons besides their charge (*spintronics*).

Many ferromagnetic objects do not show a net magnetization without an external magnetic field. This is a consequence of magnetic domains, which are formed to reduce the energy connected with the dipolar fields (the stray field and demagnetizing field). When an external magnetic field is applied domains gradually vanish due to the motion of domain walls and rotation of the magnetization inside the domains. These processes are partly reversible and irreversible. In sufficiently high fields *technical saturation* is achieved. The corresponding *saturation magnetization*, however, must not be mistaken for the *spontaneous magnetization*. The reason is that, at any temperature $T > 0$, an external field will increase the magnetization above the spontaneous value inside the domains (i. e. M_S at $H = 0$) by suppression of spin waves (the *para-process*). Hence, the experimental determination of the spontaneous magnetization in general requires a specific extrapolation of high-field data to zero field.

Spin-wave excitations are the reason for the decrease of the spontaneous magnetization with increasing temperature, which in general follows Bloch's law, i. e. the decrease of the spontaneous magnetization from its ground-state value at $T = 0$ is proportional to $T^{3/2}$. The phase transition from long-range ferromagnetic order to the paramagnetic state at a critical temperature (the *Curie temperature*, T_C) is governed by power laws for the spontaneous magnetization close to T_C, $M_S = A(1 - T/T_C)^{\beta}$, for the magnetic susceptibility, $\chi = \chi_0(1 - T/T_C)^{-\gamma}$ and for other quantities. The *critical exponents* (β and γ) are of universal character and depend only on the dimensionality of the sample in real space (e.g. 3-D for a bulk material, or 2-D for ultrathin films) and in spin space (e.g. 3-D if all orientations of the magnetization are allowed, 2-D if the magnetization vector is confined to a plane, and 1-D in the case of extremely strong uniaxial anisotropy).

In general, the magnetization of a ferromagnetic object is preferentially oriented along certain axes that correspond to an *energy minimum*, which are known as *easy axes* of magnetization. The directions of the respective *energy maxima* are called *hard axes* or *hard directions*. This property, *magnetic anisotropy*, is the key to many technical applications of ferromagnetic materials; e.g. a binary memory element requires a *uniaxial anisotropy* characterized by two stable states. The strength of the anisotropy is expressed by anisotropy constants K_i; it can be measured by the external field required to rotate the magnetization from an easy direction to a hard one. Materials with small/large anisotropy constants are called *magnetically soft/hard.*

Two interactions are responsible for magnetic anisotropies: *dipolar interactions* between atomic moments are directly connected with the shape of a given ferromagnetic body (*shape anisotropy*), while *spin–orbit interaction* is the origin of all other anisotropies: magneto-crystalline, magneto-elastic, surface/interface anisotropies, which are intimately related to the local symmetry of the atomic configuration.

10.1.2 Antiferromagnetism, Ferrimagnetism and Noncollinear Magnetism

In certain materials atomic moments are strictly ordered without showing any resulting magnetization. This happens if neighboring magnetic moments are antiparallel to each other due to a *negative exchange interaction* between the spins; this phenomenon is called *antiferromagnetism* and is mainly found in transition-metal oxides, halides etc. (MnO, CoO, NiO, α-Fe_2O_3 etc.), but also in metal alloys such as FeMn or IrMn. Antiferromagnetism vanishes above a critical temperature called the Néel temperature. Due to their zero net magnetic moment, antiferromagnets are hardly affected by external magnetic fields. This has recently led to technical applications in so-called *spin-valves* where the antiferromagnet pins the magnetization of an adjacent ferromagnetic layer in a magneto-resistive sensor.

A special form of antiferromagnetism is observed in metallic chromium: the local magnetization varies sinusoidally along certain lattice directions. This is called a *spin-density wave* and is not always commensurate with the crystal lattice.

Ferrimagnetism is a more general version of antiferromagnetism: neighboring moments are antiparallel but of different sizes, resulting in a finite net magnetization. It is found in compounds of 3d transition metals and rare-earth elements (e.g. ferrites, garnets, amorphous 3d–4f alloys and multilayers).

Other forms of magnetic order are found mainly in rare-earth compounds: magnetic moments can form helical structures (*helimagnetism*) and even more complex structures giving rise to noncollinear magnetism meaning that magnetic moments are not aligned along a defined axis. Such a magnetic order can result from different or competing exchange interactions and very strong magnetic anisotropies.

Competing ferromagnetic and antiferromagnetic coupling between neighboring moments in a crystalline lattice or purely antiferromagnetic interactions on a triangular lattice can lead to *frustration*; this means that the individual spins cannot follow the exchange cou-

pling to all neighbors simultaneously. The consequence is a spin configuration similar to a *frozen paramagnet* called a *spin-glass* state. It manifests itself by thermal hysteresis below the freezing temperature and pronounced relaxation effects, indicating the presence of highly degenerate states. Typical materials showing such behavior are dilute alloys of 3d metals (Mn, Fe, Co) in a nonmagnetic matrix (Au, Cu).

10.1.3 Intrinsic and Extrinsic Properties

Intrinsic magnetic properties are those characteristic of a given material (e.g. spontaneous magnetization, magneto-crystalline anisotropy constant etc.), while extrinsic properties are strongly affected by the specific shape and size of the magnetic object as well as by their microstructure. The most important example is the *magnetic shape anisotropy* caused by the dipolar energy via the demagnetizing field: for a three-dimensional ferromagnetic object characteristic quantities such as the remanent magnetization and saturation field are mainly determined by the shape and much less by the intrinsic magnetic anisotropy.

Another *extrinsic* effect is the role of mechanical strain in a specimen; this may be introduced during the production process. Stress and strain may significantly alter the shape of the magnetization loop via magnetostrictive effects.

10.1.4 Bulk Soft and Hard Materials

The *magnetic softness* or *magnetic hardness* of a material is a key factor for many applications. For instance, *magnetically soft* materials are needed for transformers, motors and sensors, i. e. where the magnetization should fully align with even very small external magnetic fields. This requires very low coercivity and the highest possible susceptibility (or permeability), which is equivalent to weak anisotropy and large magnetization. Also, very low magnetostriction is needed to prevent mechanical strain from building up magneto-elastic anisotropies. As an example, in some specific binary or ternary alloys of 3d metals the magneto-crystalline anisotropy can be very close to zero, making them magnetically very soft. In particular, $Ni_{81}Fe_{19}$ (*permalloy*) has nearly zero magneto-crystalline anisotropy and very weak magnetostriction. A large number of special alloys of Fe, Co and Ni with the addition of Cr, Mn, Mo, Si and other elements have been developed that allow for a compromise between high permeability (e.g. 78 permalloy = $Fe_{21.2}Ni_{78.5}Mn_{0.3}$, supermalloy = $Fe_{15.7}Ni_{79}Mn_{0.3}Mo_5$, mu-metal = $Fe_{18}Ni_{75}Cr_2Cu_5$) and high magnetization (e.g. permendur = $Fe_{49.7}Co_{50}Mn_{0.3}$). For all these alloys proper heat treatment is essential for optimum soft magnetic properties.

For high-frequency applications soft magnetic ferrites still play an important role.

Magnetically hard materials, in turn, are needed for permanent magnets, magnetic information-storage media (memories) and other applications. They should posses strong anisotropies and large coercivity so their magnetic state cannot be easily altered by external magnetic fields. Besides high coercivity and large remanent magnetization their maximum energy product $(BH)_{max}$ is a key quantity. While alloys of 3d metals with aluminum dominated the marked until 1975 (e.g. Alnico V = $Al_8Ni_{14}Co_{24}Fe_{51}Cu_3$) they have gradually been replaced by materials based on intermetallic rare-earth cobalt compounds (e.g. $SmCo_5$, $Sm_2(Co, Fe)_{17}$) and more recently by $Nd_2Fe_{14}B_1$, which does not contain relatively expensive cobalt. The magnetic properties of these materials critically depend on the metallurgical production process, which affects the granular structure needed for high coercivity and large energy product; the latter has increased by more than an order of magnitude since the development of rare-earth-containing permanent magnets. For less-demanding applications ferrite magnets are still in use.

For magnetic recording media (mainly hard-disk drives) somewhat different requirements have to be met. Here alloys of the type CoCrPt in the form of thin films are mainly used today.

10.1.5 Magnetic Thin Films

For several reasons ferromagnetic thin films constitute a special class of magnetic materials.

1. The reduced dimensionality of a thin film makes the axis perpendicular to the film plane a natural symmetry axis, which gives rise to specific magnetic anisotropies, e.g. the so-called shape anisotropy with an easy plane and a perpendicular hard axis.
2. The reduced dimensionality also causes modifications of fundamental magnetic properties such as the saturation magnetization, its temperature dependence, the Curie temperature and others. These *size effects* become more pronounced with decreasing film thickness.
3. Magnetic properties at surfaces and interfaces are generally different from the corresponding bulk

properties. These *surface effects* become more influential with decreasing film thickness and may even become dominant for *ultrathin* films, i. e. films of only a few atomic layers. Indeed, new materials with a combination of properties that does not occur in nature can be created in this way, e.g. multilayers or superlattices of a ferromagnetic and a nonmagnetic component.

4. Certain magneto-transport phenomena such as the *giant magneto-resistance* (GMR) or *tunnel magneto-resistance* (TMR) effects can best be observed and exploited in very thin films. As these effects find more practical applications (e.g. in hard-disk read heads) thin and ultrathin magnetic films receive increasing attention.

The growing interest in magnetic films and their technical application naturally increases the demand for methods and instruments to characterize their magnetic properties as completely as possible. Established instruments suitable for the study of bulk magnetic materials are of limited value because of the high sensitivity required for measurements of the small material quantities typical for thin films. Suitable methods will be described in Sect. 10.4.

10.1.6 Time-Dependent Changes in Magnetic Properties

Ferromagnetic materials frequently show a continuous change of their macroscopic magnetization in the course of time even in a constant or zero applied magnetic field. This is usually termed the *magnetic aftereffect* or *magnetic viscosity* and may occur on a time scale of seconds, minutes or even thousands of years. The underlying physical reason is that a ferromagnetic object with a net magnetic moment in the absence of an external magnetic field is generally in a thermodynamically metastable state. This is indicated by the presence of hysteresis. The equilibrium state will be asymptotically approached by domain nucleation and wall motion. Domain-wall motion is a relatively slow process due to the effective mass or inertia that can be attributed to a magnetic wall; since it is thermally activated it also depends strongly on temperature. For the same reason the coercivity of a sample depends on the measurement time if magnetization reversal occurs via domain walls. This needs to be taken into account when comparing data obtained by quasistatic measurements with those extracted from high-speed measurements (Sect. 10.3.3).

In the absence of domains walls and for a uniformly magnetized sample the magnetization responds to the torque exerted by an external magnetic field by a precession of the magnetization vector around the effective field, which is well described by the Landau–Lifschitz–Gilbert equation. As a consequence, in these cases the maximum rate of change of the magnetization is limited by the precession frequency of the magnetization vector, which for common materials like Fe, Co, Ni and their alloys is between 1 GHz and 20 GHz in moderate applied magnetic fields. It is evident that magnetization dynamics on a timescale of nanoseconds and below is relevant for magnetic devices in high-frequency applications.

10.1.7 Definition of Magnetic Properties and Respective Measurement Methods

The most important magnetic quantities are defined in the following in conjunction with their primary measurement methods.

The *magnetic field* H, or *flux density* B, (which are equivalent in free space) are measured with Hall probes, inductive probes (e.g. flux-gate magnetometers for very low fields) or nuclear magnetic resonance (NMR) probes for very high accuracy.

Magnetic moments are measured by different types of magnetometers.

- Via the force exerted by a magnetic field gradient (e.g. Faraday balance, or alternating gradient magnetometer (AGM))
- Via the voltage induced in a pickup coil by the motion of the sample, e.g. the vibrating-sample magnetometer (VSM, Fig. 10.7) is a widely used standard instrument, or a superconducting quantum interference device (SQUID, Figs. 10.48, 10.49) magnetometer for highest sensitivity

Quantity	Symbol	Unit
Magnetic field	H	[A/m]
Magnetic flux density, magnetic induction	B	[T]
Magnetic flux	Φ	[Wb]
Magnetic moment	m	[A m^2]
Magnetization ($= m/V$)	M	[A/m]
Magnetic polarization ($= \mu_0 M$)	J	[T]
Susceptibility ($= M/H$)	χ	[−]

The (average) *magnetization* of a magnetic object is usually determined by dividing the magnetic moment by the volume of the sample. Care must also be taken concerning the vector component of the magnetic moment that is detected. This is crucial in the case of samples with a significant magnetic anisotropy which can even result from the shape of the specimen (Sect. 10.1.1).

All these instruments need careful calibration. This is important because the effective calibration factors depend more or less on the size and shape of the specimen.

Magnetic moments related to different chemical elements in a specimen can be measured selectively by means of magnetic x-ray circular dichroism (MXCD) or XMCD based on the absorption of circularly polarized x-rays from a suitable synchrotron radiation source. In principle, this method allows the separation of orbital and spin magnetic moments.

If only the relative value of the magnetization is of interest and not its absolute value, then a number of different methods can be used to measure, for instance, M as a function of temperature or of the applied magnetic field. Such methods include magneto-optic effects (e.g. the magneto-optic Kerr effect (MOKE)) or the magnetic hyperfine field measured by using the Mößbauer effect, perturbed angular correlations (PAC) of gamma emission, or nuclear magnetic resonance (NMR). While MOKE is frequently used for characterizing magnetic materials, nuclear methods due to their relative complexity are restricted to special applications where standard techniques do not provide adequate information. NMR is widely exploited in magnetic resonance imaging (MRI) as a diagnostic tool in medicine.

The methods most commonly used for characterizing different magnetic materials are discussed in the following sections.

10.2 Soft and Hard Magnetic Materials: (Standard) Measurement Techniques for Properties Related to the $B(H)$ Loop

10.2.1 Introduction

During the past 100 years many different methods have been developed for the measurement of magnetic material properties and sophisticated fixtures, yokes and coil systems have been designed. Many of them vanished when new materials required extended measuring conditions. With progress in electronic measuring techniques other instruments were superseded. Fluxmeters and Hall-effect field-strength meters, for example, replaced ballistic galvanometers and rotating coils. Comprehensive explanations of the older methods can be found in [10.2]. New methods are ready to enter magnetic measuring technique. One new opportunity is for the pulse field magnetometer (PFM), which is discussed in Sect. 10.3. This device can complement the capabilities of a hysteresisgraph for hard magnetic materials, although it should be mentioned that the instrumentation is not less demanding. The difficulties involved require a careful interpretation of the results.

Table 10.1 gives an overview of the measuring methods described in the subsequent chapters. The techniques are classified according their main application for hard or soft magnetic materials, although some of them may also be applicable in the other group.

Table 10.2 compares the capabilities of various methods. Of course, it can only cover typical configurations and applications and give rough indications. In many cases, the measuring conditions may be adjusted to meet special demands. The magnitude of the quantities, which limit the measuring ranges, can either be determined by the instrumentation or by the requirements resulting from the specimen properties.

The tables can certainly not give a complete survey of all requested quantities and methods that are used today. The selected techniques are common in industrial and scientific research or in quality control.

Some basic methods in magnetic measurement are taken as known. Fluxmeters are used in many measuring set ups to integrate voltages that are induced in measuring coils to obtain the magnetic flux. Today various analog or digital integration methods are used. A discussion of them can be found in [10.3].

The same applies for field-strength meters that use the Hall effect. These instruments, usually called Gauss- or Teslameters, are widespread. A description of their working principle is given in many educational books.

In many cases it is impossible to determine the material properties of components in a shape that is defined by the production conditions or application. In these cases, relative measuring methods are often applied. These usually compare measurable properties or combinations of properties with those of a reference sample.

Sections 10.2.2 and 10.2.3 focus on methods that provide directly material properties, allow traceable

Table 10.1 Measuring methods for properties of magnetic materials

Measuring method	Soft/hard	Quantities
Hysteresisgraph for hard magnetic materials	H	$J(H)$, $B(H)$, B_r, H_{cJ}, H_{cB}, $(BH)_{max}$, μ_{rec}
Vibrating-sample magnetometer (VSM)	H, (S)	J_s, $J(H)$, B_r, H_{cJ}, H_{cB}, $(BH)_{max}$, μ_{rec}, $J(T)$, T_C
Torque magnetometer	H, (S)	Anisotropy constants
Moment-measuring coil (Helmholtz)	H	J (at working point)
Pulse field magnetometer (PFM) (Sect. 10.4)	H	J_s, $J(H)$, $B(H)$, B_r, H_{cJ}, H_{cB}, $(BH)_{max}$
DC hysteresisgraph for soft magnetic materials – ring method	S	J_s, $B(H)$, B_r, H_{cB}, $\mu(H)$, μ_i, μ_{max}, P
DC hysteresisgraph (permeameter) for soft magnetic materials – yoke methods	S	J_s, $J(H)$, $B(H)$, B_r, H_{cJ}, H_{cB}, μ_i, μ_{max}, P
Coercimeter	S, (H)	H_{cJ}
AC hysteresisgraph – ring method	S	$B(H)$, B_r, H_{cB}, μ_a, P_w, $\mu_a(H)$, $\mu_a(B)$, $P_w(H)$, $P_w(B)$, $P_w(f)$, J_s
Epstein frame	S	P_w, $J(H)$, B_r, H_{cJ}, μ_a
Single-sheet tester (SST)	S	P_w, $J(H)$, B_r, H_{cJ}, μ_a
Wattmeter method	S	P_w
Voltmeter–ammeter method	S	P_w, μ_a
Saturation coil	S	J_s, μ_r
Magnetic scales (Faraday, Gouy)	S	$\mu(H)$, μ_i, μ_{max}, $\chi(H)$, χ_i, χ_{max}, J_s, T_C
Impedance bridges	S	$\underline{\mu} = \mu' - i\mu''$, Q, $\tan\delta$

$J_s = \mu_0 M_s$ saturation polarization; T_C: Curie temperature; $B_r = J_r$: remanence; H_{cJ}: coercivity (coercive field strength) for $J(H)$ hysteresis loop; H_{cB}: coercivity (coercive field strength) for $B(H)$ hysteresis loop; $(BH)_{max}$: maximum energy product; $\mu = \mu_0\mu_r$: permeability; $\chi = \mu - 1$: susceptibility; μ_r: relative permeability; μ_i, χ_i: initial permeability/susceptibility; μ_{max}, χ_{max}: maximum permeability/susceptibility; μ_{rec}: recoil permeability; μ_a: amplitude permeability; $\underline{\mu} = \mu' - i\mu''$: complex permeability; P: hysteresis loss; P_w: total loss; Q: Q-factor, quality factor; δ: loss angle; f: frequency

Table 10.2 Characteristics of measuring methods for magnetic materials

Measurement principle	Measurement range (limiting quantities)	Measurement sensitivity	Measurement reproducibility range (%)	Materials specimen type	Specimen geometry, dimensions	Methods merit	Methods demerit
Hysteresisgraph for hard magnetic materials	H_{max}: 1.6–2.4 MA/m J_{max}: 1.2–1.5 T	H: 0.1 kA/m J: 1 mT	H: 1–3 J: 0.5–2	Bulk permanent magnets	Cylinders, blocks, segments, (large) rings	Many quantities, standardized, easy operation	Restricted for non-plane-parallel specimens
Vibrating-sample magnetometer (VSM)	H_{max}: 1.2–4 MA/m m_{max}: 1 A m^2 j_{max}: 10^{-6} V s m	H: 0.1 kA/m m: 10^{-9} A m^2, j: 10^{-15} V s m	H, J: 1–3	Ferro- and paramagnetic material, amorphous or nanocrystalline alloys	Powders, thin films, ribbons, small massive samples	High sensitivity, wide specimen temperature range	Demagnetization factor to be considered
Torque magnetometer	H_{max}: 0.8–10 MA/m L: 10^{-4}–10^{-2} N m	1) L: 10^{-9}–10^{-7} N m	1) L: 1–5	Ferro- and paramagnetic material	Discs, spheres, small particles, films, single crystals	High sensitivity, low temperatures possible	Restricted specimen shape, sometimes delicate instrumentation

Table 10.2 (continued)

Measurement principle	Measurement range (limiting quantities)	Measurement sensitivity	Measurement reproducibility range (%)	Materials specimen type	Specimen geometry, dimensions	Methods merit	Methods demerit
Moment-measuring coil	j_{max}: 10^{-4}–10^{-2} V s m	j: 10^{-10} V s m	j: 0.5–1	Bulk permanent magnets	Cylinders, blocks, rings, segments	Fast and accurate, standardized	Only for two pole magnets, one quantity
Pulse field magnetometer (PFM)	H_{max}: 4–8 MA/m	H: 1 kA/m J: 1 mT	H, J: 1–3	Bulk permanent magnets	Cylinders, blocks, segments	High field strength, fast	Demagnetization factor, eddy currents to be considered
DC hysteresisgraph – ring method	H_{max}: 10–20 kA/m	H: 0.01 A/m	H: 1 J: 1–2	Ferromagnetic, sintered or powder compacted rings, wound ring cores	Rings (geometries with closed magnetic path), stamped stacks of sheet	Many quantities, very low field strength possible, standardized	Requires specimen winding
DC hysteresisgraph – yoke methods	H_{max} : 50–200 kA/m	H: 1 A/m	H: 2–3 J: 1–2	Ferromagnetic steel	Bars, strips of sheet	Many quantities, standardized	Restricted specimen dimensions and shapes
Coercimeter	H_{max}: 20–200 kA/m	H: 0.5–1 A/m	H_c: 2–5	Ferromagnetic steel	Components of various shapes	Various specimen shapes, standardized	Only one quantity (H_c)
AC hysteresisgraph – ring method	f: 10 Hz–1 MHz	H: 0.01 A/m	J: 1–10 H: 1–2	Ferromagnetic materials	Rings (geometries with closed magnetic path), stamped stacks of sheet	Many quantities, standardized	Restricted specimen shape, requires specimen winding
Epstein frame	f: ≤ 400 Hz $\hat{J}_{max}$: 1.5–1.7 T	J: 1 mT	J: 2–3 P_w: 2–7	Ferromagnetic (electric) steel	Strips of sheet	Standardized, widespread method	Demanding specimen preparation, systematic error
Single-sheet tester (SST)	f: 50–400 Hz $\hat{H}_{max}$: 1–10 kA/m $\hat{J}_{max}$: 0.8–1.8 T	J: 1 mT	J, H: 2–3 P_w: 1–2	Ferromagnetic (electric) steel	Sheet	Standardized, simple specimen preparation	Large specimens in standardized version, systematic error
Wattmeter method	$\hat{H}_{max}$: 1–10 kA/m	2)	2)	Ferromagnetic (electric) steel	Rings, sheet using fixtures	Standardized method	Few quantities
Voltmeter–ammeter method	$\hat{H}_{max}$: 1–10 kA/m	2)	2)	Ferromagnetic (electric) steel	Rings, sheet using fixtures	Fast, standardized method, common instrumentation	Few quantities

Table 10.2 (continued)

Measurement principle	Measurement range (limiting quantities)	Measurement sensitivity	Measurement reproducibility range (%)	Materials specimen type	Specimen geometry, dimensions	Methods merit	Methods demerit
Saturation coil	H: 100–900 kA/m j_{max}: 10^{-4}–10^{-2} V s m	j: 10^{-10} V s m	j: 1–2	Nickel, Ni alloys, Co content in hard metals	Discs, wire, cylinders, small components	Fast, standardized method	Only one quantity, J_S limit depends on shape
Faraday scale	H: 800–1600 kA/m	1)	1)	Ferro-, para- and diamagnetic materials	Small massive samples, powders, films	High sensitivity, wide temperature range, small samples	Delicate, costly instrumentation
Gouy scale	H: 800–2400 kA/m	1)	1)	Para- and diamagnetic materials	Bars, vessels with liquids or gasses	High sensitivity, wide temperature range	Often delicate instrumentation, large specimen volume
Impedance bridges	f: 1 Hz–100 MHz	2)	2)	Ferro- and ferrimagnetic materials	Rings, components	Component testing close to electrical application	Require specimen winding

1) mostly research instruments with differing ranges, sensitivities and reproducibility
2) strongly depending on capabilities of standard electrical instrumentation

calibrations and are widespread in application. The information is selected to allow an evaluation of the methods. More details are given where errors are liable to be introduced.

Section 10.2.3 is completed by a short description of measuring methods for magnetostriction and, provided by Grössinger, nonstandard testing methods for soft magnetic materials that are used in scientific research laboratories.

10.2.2 Properties of Hard Magnetic Materials

Hysteresisgraph for Hard Magnetic Materials

A very important instrument for the characterization of bulk permanent magnets is the hysteresisgraph. It is mainly used to record the second-quadrant hysteresis loop. From this, material parameters such as the remanence B_r, the maximum energy product $(BH)_{max}$ and the coercive field strengths (coercivities) H_{cJ} and H_{cB}, can be determined. A measurement of recoil loops allows the calculation of the recoil permeability μ_{rec}.

The main components are an electromagnet to magnetize and demagnetize the specimen, measuring coils for the field strength H and the polarization J and two electronic integrators (fluxmeters) to integrate the voltages induced in the coils. A typical configuration of a computer-controlled hysteresisgraph is shown in Fig. 10.2.

An electromagnet with a vertical magnetic-field direction is used. The magnet specimen is placed on the pole cap of the lower pole. The upper pole can be lowered to close the magnetic circuit.

While recording the hysteresis loop, high flux densities are only required for relatively short time periods. Therefore it is possible to avoid active cooling of the electromagnet coils up to a peak electric power of approximately 3 kW. If the electromagnet is designed carefully, maximum flux densities of 1500–2400 kA/m can be achieved for specimen heights of several millimeters. Beyond this point, the steel parts of the electromagnet frame become saturated. For a further increase of the field strength significantly higher electric power and water cooling become necessary.

The measuring principle is based on the fact that the poles of the electromagnet form faces of equal magnetic potential. It is only under this condition that the specimen is homogeneously magnetized and the field strength that is measured next to the magnet is equal to its inner field strength. The pole materials (soft mag-

Fig. 10.2 Hysteresisgraph for hard magnetic materials. The cabinet contains two fluxmeters for H and J measurement and the electromagnet power supply. The specimen and surrounding coil are placed between the poles of the electromagnet (Permagraph C Magnet-Physik Dr. Steingroever GmbH, Köln)

netic steel or iron-cobalt alloy) and the polarizations of permanent-magnet specimens limit the measuring range of the method to about $H < 800\,\mathrm{kA/m}$ in the first quadrant and $|H| < 2400\,\mathrm{kA/m}$ in the second quadrant of the hysteresis loop.

As it is impossible to saturate rare-earth permanent magnets (Sm-Co, Nd-Fe-B) in an electromagnet, it is necessary to saturate them in a pulsed magnetic field prior to the measurement. Depending on the recoil permeability, the polarization will be lower than the remanence after the specimen has been inserted into the electromagnet and the magnetic circuit has been closed. However, a magnetization in the electromagnet allows full remanence to be achieved again.

Measuring Coils. Two types of measuring coils are used: the J-compensated surrounding coil and the pole-coil measuring system.

The J-compensated surrounding coil (Fig. 10.1) is suitable for all kinds of permanent-magnet materials. For the measurement it is placed around the specimen. It consists of the following windings.

One winding with area-turns of N_1A_1 encloses the inner hole of the coil that accepts the specimen during the measurement. This senses the magnetic flux penetrating the magnet specimen,

$$\Phi_\mathrm{M} = B_\mathrm{M} N_1 A_\mathrm{M}\,, \tag{10.1}$$

where B_M is the flux density and A_M is the cross-sectional area of the magnet specimen. If the coil is not completely filled by the specimen, the air flux between the specimen and the winding,

$$\Phi_{A_1} = \mu_0 H N_1 (A_1 - A_\mathrm{M})\,, \tag{10.2}$$

is also detected, where H is the field strength in air next to the specimen.

A second coil with area-turns N_2A_2 also surrounds the specimen but does not enclose it. This senses only the air flux,

$$\Phi_{A_2} = \mu_0 H N_2 A_2\,. \tag{10.3}$$

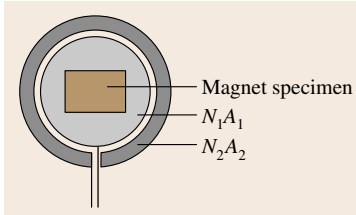

Fig. 10.1 Area-turns of a J-compensated surrounding coil

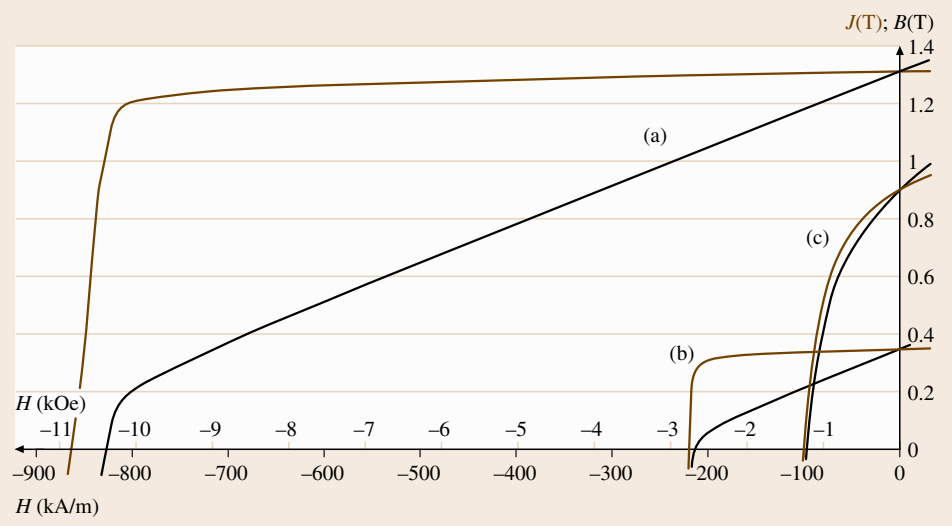

Fig. 10.3 Surrounding coil measurements on (a) NdFeB 320/86, (b) hard ferrite 24/23 and (c) AlNiCo 38/10 permanent magnets

The area-turns of the two coils are adjusted to be equal

$$N_1 A_1 = N_2 A_2 \,. \tag{10.4}$$

Both coils are connected in series opposition to a fluxmeter integrator. If the inner of the first coil is partially filled by a specimen, the magnetic flux measured is

$$\begin{aligned}\Phi &= \Phi_{\mathrm{M}} + \Phi_{A_1} - \Phi_{A_2} = (B_{\mathrm{M}} - \mu_0 H) N_1 A_{\mathrm{M}} \\ &= J N_1 A_{\mathrm{M}} \,,\end{aligned} \tag{10.5}$$

where J is the polarization of the specimen, which is connected to the magnetization M by $J = \mu_0 M$. In the absence of a specimen the resulting flux Φ is zero.

Usually the surrounding coil system contains a third coil that senses the magnetic field strength H. It is connected to a second fluxmeter integrator. In this way the $J(H)$ hysteresis loop can be measured directly using one combined-coil system that can be made 1 mm thin. The $B(H)$ hysteresis loop can be derived from the $J(H)$ loop. Figure 10.3 shows the demagnetization curves of different permanent-magnet materials measured using surrounding coils.

Instead of the field measuring coil a Hall probe can also be placed next to the specimen to sense H. This requires additional space for the probe and an additional measuring instrument. Because of the linearity error and the temperature dependence of the sensitivity of a Hall sensor, suitable corrections are necessary. Additional errors can arise from the facts that the Hall probe always has to be aligned truly perpendicular to the magnetic-field direction and that it is, due to the small active area, more sensitive to local field-strength variations.

The second coil system that is used in hysteresisgraphs is the pole-coil measuring system [10.4]. It is used mainly for hard ferrite magnets. The pole-coil system consists of two coils that are embedded into one pole of the electromagnet (Fig. 10.4). One coil is completely covered by the specimen. The other coil remains free.

The first coil senses the flux density B at the surface of the specimen. The second coil measures the magnetic field strength H. Both coils are connected in series opposition. In this way the polarization, $J = B - \mu_0 H$, is obtained directly. This compensation also cancels out the residual field of the poles before the specimen is inserted.

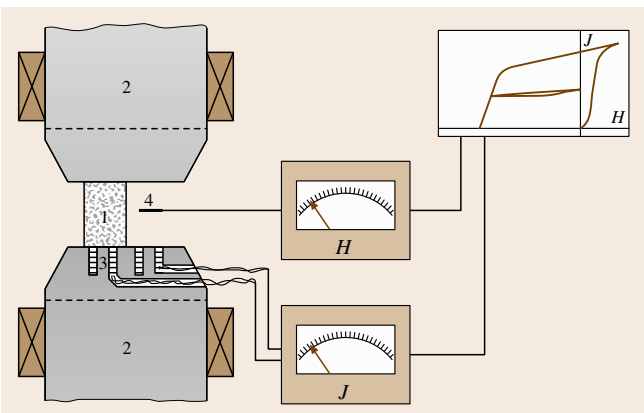

Fig. 10.4 Hysteresis measurement with pole coils (1 – magnet specimen, 2 – electromagnet poles, 3 – pole coils, 4 – field-strength sensor)

Fig. 10.5 Segment poles with pole coils

The surrounding coil measures the whole magnetic flux penetrating the specimen. The pole-coil system only senses the flux in a small area (typically with a diameter of 3–6 mm) on the surface. Therefore it is suitable for the detection of nonhomogeneities in different regions. Especially for anisotropic ferrite magnets it is usual to carry out measurements on both sides of a magnet to quantify differences caused by the production process.

Pole-coil systems are also made arc-shaped for measurements on segment magnets for motor applications. They must be machined to match the radii of the segments exactly. Both the upper and the lower pole contain a pair of pole coils.

Measurements at Elevated Temperatures. For measurements at temperatures up to 200 °C pole caps with built-in heating (Fig. 10.6) can be used. A hole in the pole cap accepts a thermocouple for temperature measurement and control. Prior to the measurement the specimen must remain between the poles for a sufficient time to reach the desired temperature. The surrounding coil needs to be temperature-proof. Hysteresis measurement is carried out in the same way as at room temperature.

Measurements on Powders. Powder samples can be measured in the same way as solid magnets if the powder is filled into a nonmagnetic container, for example a brass ring that is sealed with a thin adhesive foil at the bottom. As the measured polarization depends on the apparent density, it may be more feasible to regard the specific polarization. The coercivity H_{cJ} however can be measured directly.

Vibrating Sample Magnetometer (VSM)

The VSM is used to measure the magnetic moment m and the magnetic dipole moment $j = \mu_0 m$ in the presence of a static or slowly changing external magnetic field [10.5]. As the measurement is carried out in an open magnetic circuit the demagnetization factor of the specimen must be considered.

Most instruments use stationary pickup coils and a vibrating specimen but arrangements with vibrating coils and rigidly mounted specimens have also been proposed. The drive is either carried out by an electric motor or by a transducer similar to a loudspeaker system.

The specimen is suspended between the poles of the electromagnet and oscillates vertically to the field direction; it must be carefully centered between the pickup coils.

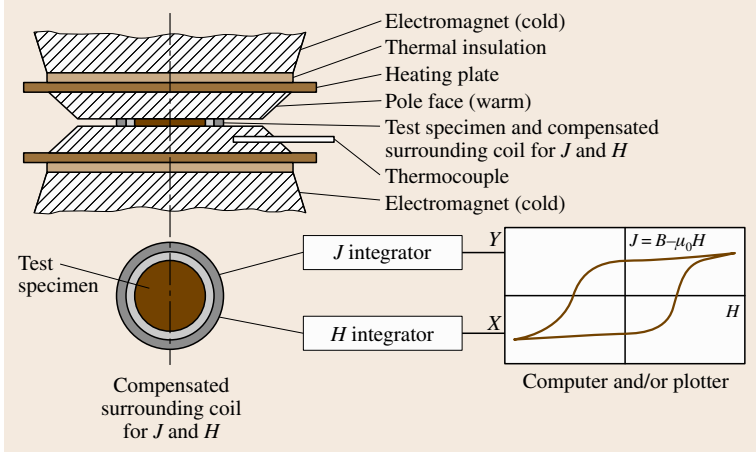

Fig. 10.6 Heating poles for measurements at elevated temperatures

In the pickup coils a signal at the vibration frequency is induced. This signal is proportional to the magnetic dipole moment of the specimen but also to vibration amplitude and frequency. The coil design ensures that it is independent of variations in the field generated by the electromagnet.

The amplitude and frequency can be measured separately, for example using

- a capacitor with one set of fixed plates and one set of movable plates (Fig. 10.7),
- a pickup coil and a permanent magnet,
- an electrooptical sensing system.

The signals are fed to a differential amplifier, so that changes of oscillation amplitude and frequency can be compensated. A synchronous detector (lock-in amplifier) followed by a low-pass filter produces a direct-current (DC) output signal that only depends on the magnetic moment.

For the generation of the outer magnetic field a strong electromagnet is required; the field direction is horizontal. Water-cooled magnets are mostly used but superconducting magnets are also common. The power required is even higher than for a hysteresisgraph as the volume between the pole caps is quite large. The specimen rod must be able to oscillate, and sufficient space for a pickup coil system is required between the specimen holder and the pole caps.

Usually a distance that is sufficient for an optional oven or a cryostat to heat or cool the specimen is chosen. Ovens, LN_2 or helium cryostats that are shaped to fit between electromagnet poles are available. Care must be taken to avoid errors due to magnetic components or electrical supply lines. In this way the determination of Curie temperatures and the observation of other phase transitions become possible.

Figure 10.8 shows measurements on nanocrystalline specimens. Measurement below room temperature was carried out using an LN_2 cryostat. Above room temperature a tubular oven was used; it had a water-cooled outer wall to avoid heating of the pickup coils and electromagnet poles. The oven can be evacuated or filled by an inert gas to avoid specimen oxidation.

For practical purposes and to separate the mechanical system from building oscillations it is usually mounted onto the electromagnet. This offers a stable base due to its large mass. For high sensitivity the transfer of oscillations from the drive to the pickup coils through the electromagnet should be avoided; a mechanical resonator can achieve this. In this case the drive frequency must be matched to the resonant frequency.

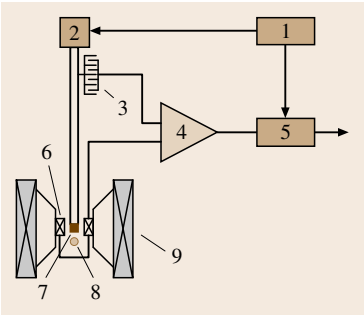

Fig. 10.7 Vibrating-sample magnetometer: 1 – oscillator, 2 – transducer, 3 – capacitor for frequency and amplitude measurement, 4 – differential amplifier, 5 – synchronous detector, 6 – pickup coils, 7 – specimen, 8 – H field sensor, e.g. Hall probe, 9 – electromagnet poles and coils (frame not shown)

A VSM is mostly used for measurements on magnetically hard or semi-hard materials. Specimen forms include small bulk samples, powders, melt-spun ribbons and thin films. The VSM can also be used for measurements on soft magnetic materials. In this case the electromagnet can be replaced by a Helmholtz-coil system.

VSMs are very sensitive instruments. Commercial systems offer measuring capabilities down to approximately $10^{-9}\,\mathrm{A\,m^2}$. A system that used a SQUID sensor instead of pickup coils achieved a resolution of $10^{-12}\,\mathrm{A\,m^2}$ [10.6].

Closely related to the VSM is the alternating gradient field magnetometer (AGM). As it is typically

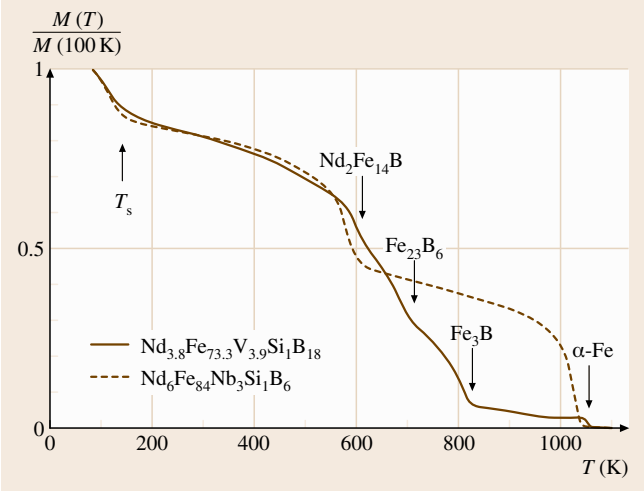

Fig. 10.8 VSM measurement of the temperature dependence of the magnetization M of nanocrystalline melt-spun samples. The *curve* shows the spin-reorientation temperature T_s of $Nd_2Fe_{14}B$ and the Curie temperatures of the comprised phases (heating curves, $dT/dt = 45\,\mathrm{K/min}$)

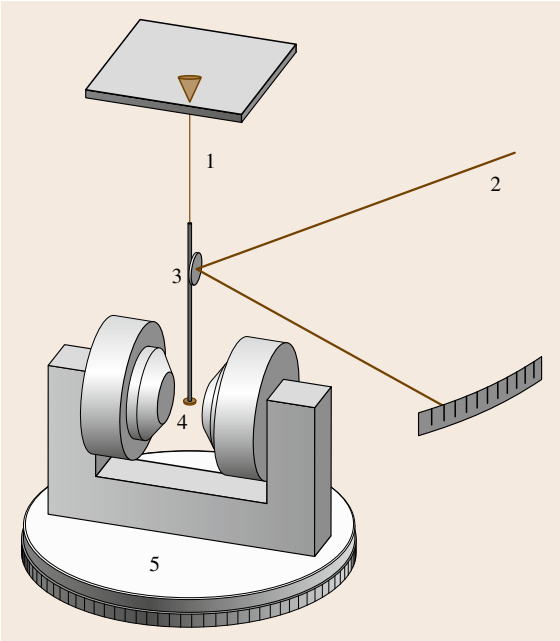

Fig. 10.9 Torque magnetometer: 1 – torsion wire, 2 – light beam, 3 – specimen rod with mirror attached, 4 – specimen, 5 – electromagnet on rotating base

used for measurements on thin films, it is discussed in Sect. 10.4.

Torque Magnetometer

If the magnetization energy of a freely rotating specimen depends on direction, the specimen aligns with its axis of easy magnetization parallel to a magnetic field. The axis of easy magnetization is determined by the magnetocrystalline anisotropy energy E_a if the specimen has rotational symmetry.

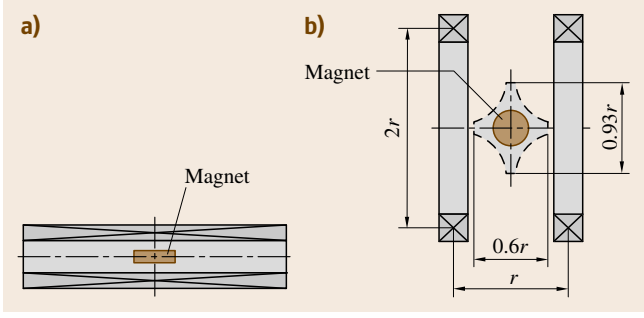

Fig. 10.10a,b Moment-measuring coils: solenoid **(a)** and Helmholtz coil. **(b)** The *dashed line* in the Helmholtz coil marks the cross section of the measuring space for 1% accuracy

If the magnetic field is rotated out of the preferred direction by an angle α, the vector of polarization J_s will point in the direction of H, if the field strength is sufficiently large to saturate the specimen. If H is smaller, the direction of J_s is rotated only by an angle $\varphi < \alpha$.

For a material showing uniaxial anisotropy, the anisotropy energy is assumed to be

$$E_a = K_1 \sin^2\varphi \,, \tag{10.6}$$

where K_1 is the uniaxial anisotropy constant. The magnetizing energy is

$$E_H = HJ_S \cos(\alpha - \varphi) \,, \tag{10.7}$$

which leads to the torque

$$L = -\frac{\mathrm{d}(E_a + E_H)}{\mathrm{d}\varphi} = -K_1 \sin 2\varphi - HJ_S \sin(\alpha - \varphi) \,. \tag{10.8}$$

Therefore the determination of anisotropy constants requires high field strengths or suitable extrapolation. A broad discussion of the anisotropy energy for different crystal symmetries can be found in [10.7, Chap. 5].

The specimen is attached to a rod that is suspended between torsion wires, and is located between the poles of an electromagnet. The electromagnet is mounted to a base plate that can be rotated by 360°. The rotation angle can be measured and recorded.

The excitation of the specimen is measured by the deflection of a light beam from a mirror that is attached to the specimen rod.

Automated systems use an electrodynamic compensation of the torsion, which is measured by an optical system consisting of a mirror attached to the specimen rod, a light beam and photosensors to detect the excitation. The excitation is compensated by an electromagnetic system that is located outside the stray field of the electromagnet. The current in the compensating coil is proportional to the torque.

The main application of the torque magnetometer is the determination of anisotropy field constants of hard magnetic materials, including small particles and thin films. Other applications are the determination of texture on grain-oriented electrical sheet and strip and the determination of the anisotropy of susceptibility of paramagnetic materials with noncubic structure.

Moment-Measuring Coils

Helmholtz-coil configurations [10.8] are very common for the measurement of the magnetic dipole moment of permanent magnets. They provide a large region with

uniform sensitivity that can be easily accessed from all sides. Long solenoids can also be used (Fig. 10.10). The installation of the coil must be carried out with care. No magnetic or magnetizable parts are allowed in the vicinity of the coil as they would affect the measurement result.

The measuring coil is connected to a fluxmeter. The magnet specimen is placed in the center of the coil so that the vector of polarization is aligned with the coil axis. The fluxmeter is set to zero and the magnet is withdrawn from the coil as long as the reading of the fluxmeter changes. Alternatively the magnet can be rotated by 180° so that the vector of polarization points in the opposite direction. If the rotation method is used, the fluxmeter reading must be divided by 2.

The magnetic dipole moment j of the specimen is proportional to the measured magnetic flux Φ,

$$j = k\Phi \,. \tag{10.9}$$

The measuring constant k can be calculated from the dimensions and the number of turns n of the coil. For a Helmholtz coil, k is approximately $1.4r/n$, where r is the coil radius. In practice, k is obtained by calibration.

From the dipole moment, the magnetic polarization J in the working point of a magnet with the volume V can be calculated using

$$J = j/V \,. \tag{10.10}$$

This allows the determination of the working point if the demagnetization curve of the material is known.

For an anisotropic magnet, the polarization in the working point is typically only 1–3% lower than the remanence B_r. This fact is used in the main application of the method: a fast and repeatable test for B_r. This makes it popular in industrial quality control if a measurement of the demagnetization curve is too time-consuming or expensive.

The method can also be used for radially anisotropic, arc-shaped magnets that are common in motor applications (Fig. 10.11). As the coil only detects the magnetic moment parallel to the coil axis, a correction must be applied.

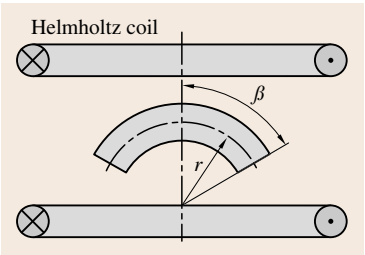

Fig. 10.11 Measurement of the magnetic dipole moment of a radially anisotropic segment magnet

The measured magnetic dipole moment is

$$j' = 2JAr \int_0^{\beta} \cos\beta \, \mathrm{d}\beta \,. \tag{10.11}$$

Here A is the cross-sectional area of the specimen. The volume of the magnet,

$$V = 2Ar\beta \,, \tag{10.12}$$

leads to the polarization

$$J = \frac{j'}{V} \frac{\beta}{\sin\beta} \,. \tag{10.13}$$

Another application is the determination of the anisotropy direction of block magnets. The magnetic dipole moment is measured in the direction of one geometrical symmetry axis (j_x) and in two perpendicular directions (j_y, j_z).

The angle α between the geometrical symmetry axis and the axis of anisotropy is

$$\alpha = \arccos \frac{j_x}{\sqrt{j_x^2 + j_y^2 + j_z^2}} \,. \tag{10.14}$$

10.2.3 Properties of Soft Magnetic Materials

DC Hysteresisgraph – Ring Method

The basic method for the measurement of quasistatic hysteresis loops mostly uses ring-shaped specimens (Fig. 10.12). Other specimen shapes providing a closed magnetic circuit with constant cross section may also be appropriate. The specimen is equipped with a primary winding and a secondary winding.

Usually the bipolar current source is computer-controlled and the fluxmeter and ammeter are also integrated into a data-acquisition system.

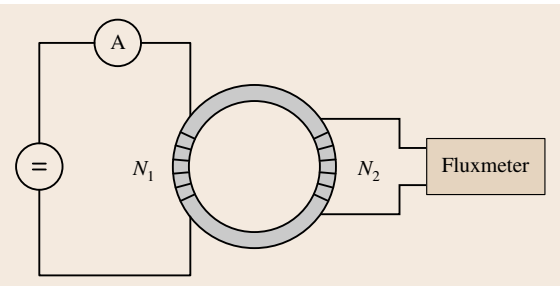

Fig. 10.12 Circuit of the ring method

The magnetizing current I is applied to the primary winding. The magnetic field strength H is calculated from

$$H = \frac{N_1 I}{l_\mathrm{m}} , \tag{10.15}$$

where N_1 is the number of turns of the primary winding. The mean magnetic path length l_m is usually obtained from

$$l_\mathrm{m} = \pi \frac{D+d}{2} , \tag{10.16}$$

where D is the outside diameter and d is the inside diameter of the ring.

The radial variation of H must be kept small. Therefore the ratio between the outer diameter and inner diameter should not exceed 1.4. Thinner rings are often impracticable, especially for fragile sintered specimens. If this condition cannot be met for any reason, l_m can better be calculated with respect to the average field strength,

$$l_\mathrm{m} = \pi \frac{D-d}{\ln\left(\frac{D}{d}\right)} . \tag{10.17}$$

The voltage that is induced into the secondary winding must be integrated to obtain the magnetic flux Φ. Therefore a fluxmeter is used. From the flux Φ, the flux density B is calculated as

$$B = \frac{\Phi}{N_2 A} . \tag{10.18}$$

Here N_2 is the number of turns of the secondary winding and A is the cross-sectional area of the specimen. For a massive ring of rectangular cross section and height h, the area is calculated from

$$A = \frac{D-d}{2} \cdot h . \tag{10.19}$$

If the ring consists of stacked sheets or wound ribbons, the area must be calculated from

$$A = \frac{2m}{\rho\pi(d+D)} , \tag{10.20}$$

where m is the mass and ρ is the density of the specimen material.

Prior to the measurement the specimen is demagnetized. An alternating current with decreasing amplitude is applied to the primary winding. The frequency and decay rate of this current can be preset. The measurement can then be started with the initial magnetization curve. The hysteresis loop is either excited up to the maximum current provided by the current source or to a preset limit of H or B.

Often the measuring speed is controlled so that a constant rate of change of the flux density with time, $\mathrm{d}B/\mathrm{d}t$, is achieved. This allows the steep parts of the loop to be passed slowly to avoid errors due to eddy currents. The flat parts of the curves can be passed faster as eddy currents do not affect the magnetization. However, the instrument must also have the possibility to run curves at constant speed, for instance in the case that control is not possible, e.g. for a high squareness loop. The typical time to trace a hysteresis loop is of the order 1 min.

Quasistatic measurement allows one to obtain magnetic material properties independently of the influence of eddy currents. In this way the hysteresis loss can be obtained directly by integrating the area of the hysteresis loop

$$P = \oint B \,\mathrm{d}H . \tag{10.21}$$

Coercivities of soft magnetic ring specimens range from less than 0.1 A/m for ring cores made of wound ribbons of amorphous alloys up to several 100 A/m for rings made of solid steel or sintered material. Depending on the ring dimensions, current and number of primary turns, typically maximum field strengths up to approximately 10 kA/m can be achieved.

The permeability curve $\mu_\mathrm{r}(H)$ can be created by dividing the corresponding values of B and $\mu_0 H$, which are usually taken from the initial magnetization curve. The highest point of the $\mu_\mathrm{r}(H)$ curve, the maximum permeability μ_max, is typically stated in measurement reports.

Figure 10.13 shows some sample measurements on different materials. The field-strength excitation is 5 kA/m for the Fe-Si and 60 A/m for the Fe-Ni specimen.

Winding a Ring Specimen. In schematic drawings such as Fig. 10.12 primary and secondary windings are usually shown on opposite sides of the ring. This configuration produces a high stray field if the permeability decreases while approaching saturation. Therefore, both windings are often equally distributed around the circumference if the number of turns is sufficiently large. To avoid air flux between the ring and the secondary winding, this winding is wound directly onto the ring. The primary winding is wound onto the secondary winding.

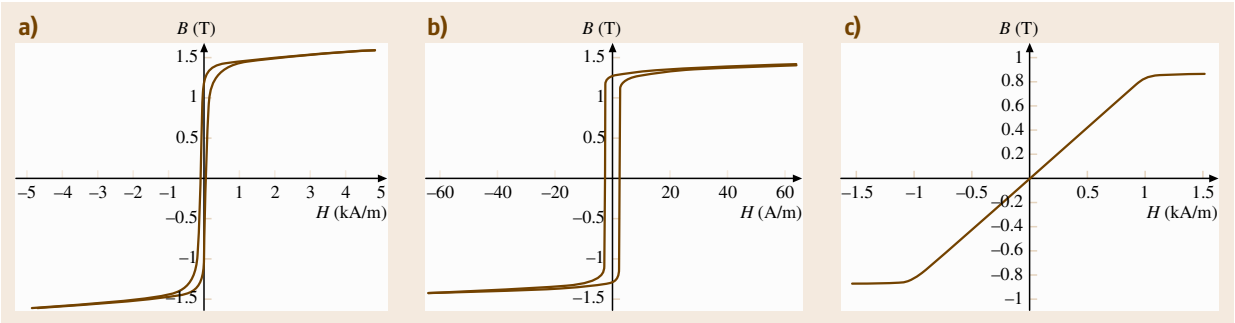

Fig. 10.13a–c Hysteresis loops of ring specimens measured by the DC ring method, **(a)** Fe-Si alloy with round (R-)hysteresis loop, **(b)** Fe-Ni alloy with high squareness (Z-)loop, **(c)** amorphous cobalt alloy with flat (F-)loop

Each of the equally distributed windings produces an effective circular turn with a diameter equal to the mean diameter of the ring. In this way the primary winding produces a magnetic field in the direction of the ring axis. This can be avoided by winding the turns in pairs of layers that are wound alternating clockwise and counterclockwise around the ring.

This also reduces the error arising from the effective mutually inductive coupling between the two windings in the axial direction. To minimize this error, the wire of the secondary winding can also be led back along the mean diameter of the ring.

After winding, the specimen should be checked for short circuits between the windings and core.

Specimens for ring-core testing include wound ribbons of amorphous alloys and iron-nickel alloys. If the magnetic properties can easily be altered by mechanical stress, the windings cannot be applied to the cores directly. The cores can be coated or placed in plastic core boxes that are wound afterwards. Prefabricated windings with multipole connectors are also used.

Depending on the field-strength range, the air flux between the measuring winding and specimen must be considered. The flux density must then be calculated from

$$B = \frac{\Phi}{N_2 A} - \mu_0 H \frac{A_2 - A}{A} , \qquad (10.22)$$

where A_2 is the cross-sectional area of the secondary winding and A is the area of the specimen.

DC Hysteresisgraph – Yoke Methods

The DC hysteresisgraph or permeameter is used for quasistatic hysteresis measurements on soft magnetic materials. The specimen can either be a bar with round or rectangular cross section or a strip of flat material. The choice of the method depends on the shape and magnetic properties of the specimen. Yoke methods are generally used instead of the ring method if the coercivity of the specimen material is larger than 50–100 A/m. Maximum field strengths range from 50–200 kA/m.

The most widespread yoke configurations today are the permeameter yokes type A and type B according to [S-10-31] and the Fahy permeameter [10.9] (Fig. 10.14). Many other, often similar, configurations have been designed. A larger collection can be found in [10.10].

For the measurement of the flux density B, a coil that is directly wound onto the specimen can be used. In everyday use J-compensated coils are often preferred. They can be made sturdier and can be used for specimens with various diameters and shapes.

The measurement of the field strength H can be carried out by a Hall probe or a field-measuring coil (search coil) next to the specimen. Due to the restricted space, this approach is used with the type A permeameter. Another way is a c-shaped potential-measuring coil, as shown in Fig. 10.14b for the type B permeameter. It is placed directly onto the specimen surface and senses the magnetic potential difference P between its ends. The magnetic field strength is obtained by $H = P/s$, where s is the distance between the ends of the potential coil. A straight potential-measuring coil can be used with the Fahy permeameter.

In the type A permeameter, the specimen is surrounded by the magnetizing coil. This configuration generates relatively high field strengths. However, specimen and field strength sensor are heated directly by the power dissipation in the coil. If the field strength is increased above approximately 50 kA/m, forced air or even water cooling becomes necessary. The minimum specimen length for the type A permeameter is 250 mm.

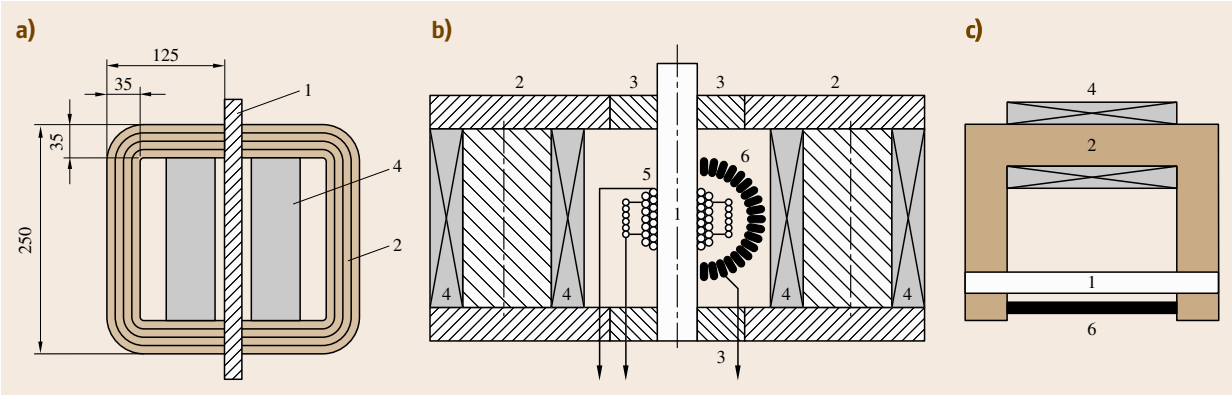

Fig. 10.14a–c Permeameters: IEC Type A (**a**), IEC Type B (**b**), Fahy Simplex (**c**). 1 – specimen, 2 – yoke frame, 3 – exchangeable pole pieces, 4 – field-generating coils, 5 – surrounding coil for B or J, 6 – sensor for H

The type B permeameter uses specimens that are only 90 mm long, but the maximum field strength is limited to 50–60 kA/m as the yoke frame saturates above.

Like in the DC ring method, the measuring speed is often controlled to $\mathrm{d}B/\mathrm{d}t = \text{const.}$ to minimize the influence of eddy currents on the measurement results.

Coercimeter. The size and shape of soft magnetic components often makes it impossible to measure the complete hysteresis loop. In this case a coercimeter can be used to determine the coercivity H_{cJ}. As this quantity depends sensitively on the microstructure, it is a good indicator of successful material heat treatment. The measurement is carried out in an open magnetic circuit.

A solenoid is used to magnetize and demagnetize the specimen. The maximum field strength must be sufficient to achieve technical saturation, beyond which the coercivity would remain constant if the magnetizing field strength were further increased. This can be tested by a series of measurements with increasing magnetizing field strengths. The required field strength depends on the specimen material and shape. Commercial solenoids provide up to 100–200 kA/m. Sometimes an additional higher-field pulse is used for saturation.

After the specimen has been saturated and the polarity is reversed, the field strength must be increased slowly to avoid errors due to eddy currents in the specimen. A field sensor detects the stray field. For a homogeneously magnetized specimen the stray field vanishes at H_{cJ}. Fluxgate probes, Hall probes or compensated coils can be used as zero-field-strength detectors. The arrangement of the sensors in Fig. 10.15 ensures that only the stray field of the specimen and not the field generated by the solenoid is measured.

Formerly it was usual to align the instrument with respect to the Earth's magnetic field. Today shielded systems are preferred as they are easier to install and also dynamic noise fields are suppressed.

It is often claimed that coercimeters allow measurement of the coercivity independently of the specimen shape. For machined components such as parts of relays the coercivity is not uniform due to mechanical or heat treatment. Complex-shaped parts are not uniformly magnetized. In these cases the coercimeter provides only an integral value given by the vanishing stray field at the sensor position.

AC Hysteresisgraph. An AC hysteresisgraph is mainly used for ring specimens but also sometimes with fixtures that allow measurements of strips. In these cases

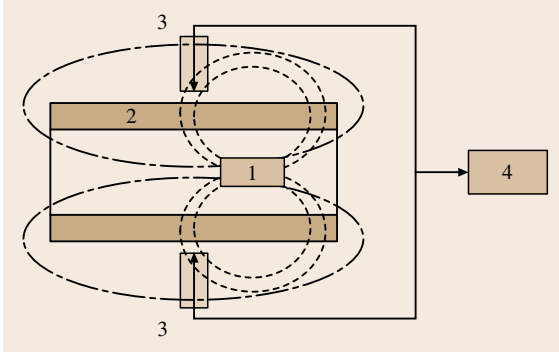

Fig. 10.15 Coercimeter: 1 – specimen, 2 – field-generating solenoid, 3 – field sensors, 4 – zero detector

the feedback yoke, e.g. a C-core, must be laminated to avoid eddy currents. The permeability should be high compared with the permeability of the specimen.

For the winding of the ring specimen the same considerations as for the DC ring method apply.

The simplest version of an AC hysteresisgraph uses an oscilloscope. The secondary induced voltage is integrated using a resistor–capacitor (RC) circuit. The output is displayed as a function of the primary current. Today this method is mainly used for demonstration purposes. For material testing, digital data-acquisition systems are more suitable.

Figure 10.16 shows the operating principle. A programmable function generator controls a power amplifier that supplies a current I to the primary winding of the specimen. The current is measured using a shunt with negligible inductance. From the current and the magnetic path length l_m the field strength H can be calculated. The secondary induced voltage is digitized and integrated to obtain the flux density B.

The measuring conditions have to be defined to achieve comparable results. Programmable function generators allow the waveform of B to be defined as sinusoidal [10.11]. A sinusoidal H can be easier achieved using a current output amplifier. Systems with digital control for B are available up to frequencies of several kHz, while uncontrolled systems can reach several 100 kHz or even a few MHz.

Due to an increase of applications for soft magnetic materials using pulse-width modulation (PWM), the interest in measuring systems that allow measurements in the presence of higher harmonics is growing [10.12]. Function generators with arbitrarily programmable waveforms can meet these requirements.

After $U_1(t)$ and $U_2(t)$ have been recorded, various evaluations can be carried out. The hysteresis loop and the total loss can be calculated.

The AC hysteresisgraph can also measure the curve of normal magnetization, also called commutation curve. Therefore the amplitude of the magnetizing current is successively increased and corresponding peak values of the field strength and flux density, $\hat{H}$ and $\hat{B}$, are recorded. The amplitude permeability $\mu_a(H)$ or $\mu_a(B)$ can be calculated from these.

Epstein Frame. The Epstein frame is mainly used by producers and users of electrical sheet and strip. Many consignments in industry are based on Epstein values. The main disadvantage of the method is the demanding specimen preparation and the large quantity of specimen material. The classical Epstein frame had a width

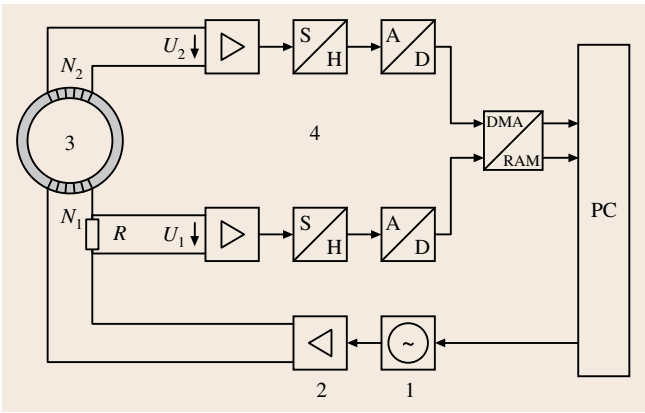

Fig. 10.16 AC hysteresisgraph: 1 – programmable frequency generator, 2 – power amplifier, 3 – specimen, 4 – transient recorder with preamplifier and analog-to-digital conversion

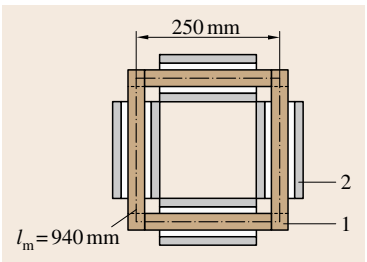

Fig. 10.17 25 cm Epstein frame: 1 – specimen, 2 – magnetizing and measuring coils

of 50 cm and required about 10 kg specimen mass. It has been nearly completely replaced by the 25 cm frame (Fig. 10.17).

Four coil sets form the frame. Each of them contains two windings: an inner flux measuring winding and an outer winding to magnetize specimen. The specimen must be cut into strips that are between 280 mm and 320 mm long and 30 mm ± 0.2 mm wide. These are stacked into the frame so that they overlap alternately in the corners.

For nonoriented material, one half of the strips is cut in the rolling direction and the other half perpendicular to it. The strips cut perpendicular to the rolling direction must be placed at opposite sides.

Measurements are mainly carried out at power-line frequencies (50–400 Hz). Rarely the Epstein frame is also used for quasistatic measurements or up to the kHz range. Normally the measurements are carried out under the condition of sinusoidal flux density B. The excitation is typically limited to $\hat{B} = 1.5$ T for nonoriented and $\hat{B} = 1.8$ T for oriented material. At higher excitations, digital or analog feedback control becomes necessary.

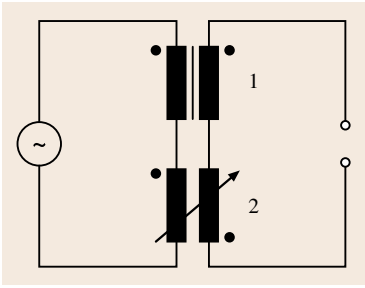

Fig. 10.18 Air-flux compensation using an adjustable mutual inductor: 1 – Epstein frame, 2 – mutual inductor

To calculate the magnetic field strength H from the magnetizing current I, the magnetic path length l_m is required (10.11). Due to the overlapping edges, l_m cannot be determined exactly. Therefore it is set by definition to 94 cm for the 25 cm frame.

To obtain the polarization J, the air flux that is generated in the measuring coils must be compensated. A mutual inductor is the conventional solution (Fig. 10.18). It is adjusted so that the output of the measuring winding is canceled out if no specimen is inserted in the frame.

Today the Epstein frame is mostly connected to a data-acquisition system, as shown in Fig. 10.16 for the AC hysteresisgraph. Then the air-flux correction can also be carried out by calculating the difference between a measurement with an empty frame and the measurement on the specimen.

The Epstein frame is not always used to measure the complete hysteresis loop. If only loss or permeability data are required, the wattmeter method or the voltmeter–ammeter method can be applied to the Epstein frame.

Single-Sheet Tester. The single-sheet tester (SST) uses a yoke to close the magnetic circuit (Fig. 10.19). The specimen is placed between the two halves of the yoke inside a set of coils that consists of an inner measuring coil and an outer coil that applies the magnetizing field.

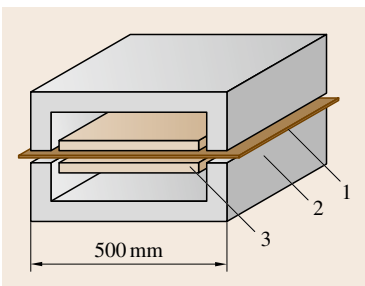

Fig. 10.19 Single-sheet tester: 1 – specimen, 2 – yoke frame, 3 – magnetizing and measuring coils

The standardized SST yoke is 500 mm long and wide. It is designed for sheets with a minimum length of 500 mm. A square specimen allows measurement in and perpendicular to the rolling direction. Narrower specimens can also be measured. For a sufficient measuring signal, they should cover at least 60% of the yoke width. In practice down-scaled frames for smaller specimen sizes are also used.

To minimize the influence of eddy currents, the frame must be made of strip-wound cut cores or stacked isolated sheets. The magnetic losses of the yoke must be much smaller than the losses of the specimen. Therefore high-quality electrical steel or iron-nickel alloy is used.

The main advantages compared to the Epstein frame are lower specimen mass and easier specimen preparation and installation. The SST allows the measurement of the same quantities and curves as the Epstein frame. The electronic part of the instrumentation is principally the same.

For comparing Epstein frame to SST measurements, it is essential to explore the relationship between the two methods [10.13]. The results of an extended comparison for grain-oriented steel are compiled in [10.14]. Unfortunately a single correlation factor for all material grades could not be established.

Normally the field strength is calculated from the magnetizing current. In this case the magnetic losses of the yoke and in the gaps to the specimen must be minimized. An uncertainty also exists in the determination of the magnetic path length. To overcome these difficulties, a measurement of the field strength has been proposed, among others by [10.15], but attempts in this direction have shown poor reproducibility.

Wattmeter Method. The wattmeter method is used to measure the specific total loss (power loss) on ring specimens at a given alternating-current (AC) excitation. The measurement is carried out under condition of sinusoidal magnetic flux density. For some specimens this may require digital control of the magnetizing current waveform or an analog feedback control of the power amplifier.

The circuit of the wattmeter method is shown in Fig. 10.20. Three instruments are necessary: a voltmeter V_1 displaying the average rectified value (sometimes scaled to 1.111 times the rectified value), a voltmeter V_2 displaying the root mean square (rms) voltage and a wattmeter. All instruments must have high input impedances and the wattmeter must have a low power factor.

Prior to a measurement the specimen must be demagnetized. Therefore the amplitude of the magnetizing alternating current is slowly reduced from its maximum value to zero. The current is then increased to generate the desired flux density $\hat{B}$ in the specimen. This is determined via the average rectified voltage

$$\overline{|U_1|} = 4 f N_2 A \hat{B} \,. \tag{10.23}$$

The form factor of the secondary waveform must be verified to ensure a sinusoidal flux density. This is determined by the ratio of the rms voltage U_2 to the average rectified voltage U_1. Additionally an oscilloscope can be used to monitor the waveform.

For the calculation of the total loss of the specimen, the power P_i consumed by the instruments connected to the secondary winding must be taken into account. As the voltage shall be sinusoidal it is, to a first approximation, equal to

$$P_\mathrm{i} = \frac{\left(1.111 \cdot \overline{|U_2|}\right)^2}{R_\mathrm{i}} \,, \tag{10.24}$$

where R_i is the combined input resistance of all the instruments connected to the secondary winding. The total loss P of the specimen is calculated from the reading P_m of the wattmeter using

$$P = \frac{N_1}{N_2} P_\mathrm{m} - P_\mathrm{i} \,. \tag{10.25}$$

The specific total loss is obtained by dividing P by the mass of the specimen.

Voltmeter–Ammeter Method. The voltmeter–ammeter method allows the determination of the normal magnetization curve and the amplitude permeability. The circuit of the method is shown in Fig. 10.21. The instruments needed are an average-type voltmeter, a root-mean-square-type (rms) voltmeter and an rms or peak-reading ammeter or a noninductive resistor and appropriate voltmeter. The voltmeters must have high input impedances. An oscilloscope can be helpful to monitor the secondary induced waveform.

If comparable results are desired, either the waveform of the primary current or of the secondary voltage must be kept sinusoidal. Depending on the excitation and the shape of the hysteresis loop control can be necessary. A sinusoidal H waveform can be achieved by a current-controlled power amplifier or by a feedback using a noninductive resistor in the primary circuit. This can be the resistor used for current measurement. A sinusoidal secondary voltage can be achieved by analog or digital control. The form factor can be determined by the ratio of the rms voltage to the average rectified voltage.

The excitation field strength $\hat{H}$ is calculated from the current I using (10.15). If I is sinusoidal it can be measured by multiplying the rms value by the square root of 2. If the primary waveform is significantly nonsinusoidal a peak-reading instrument would be required. In practice this is often ignored and an effective excitation field strength that is lower than the real field strength is used instead.

Prior to the measurement the specimen is demagnetized. Then I is successively increased and the average rectified value of the secondary voltage is measured. The flux density $\hat{B}$ is calculated from (10.23). The normal magnetization curve can be obtained by plotting corresponding values of $\hat{H}$ and $\hat{B}$.

The relative amplitude permeability μ_a can be calculated from

$$\mu_\mathrm{a} = \frac{\hat{B}}{\mu_0 \hat{H}} \tag{10.26}$$

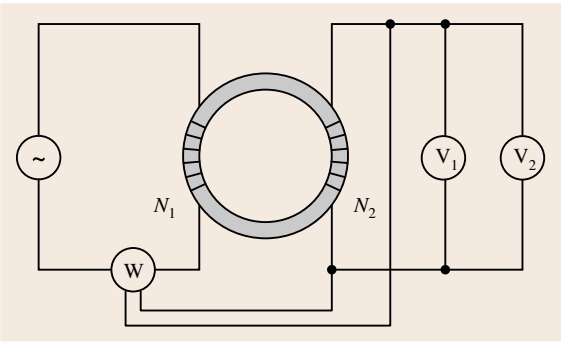

Fig. 10.20 Circuit diagram of the wattmeter method. V_1 is an average-type voltmeter, V_2 is an rms voltmeter

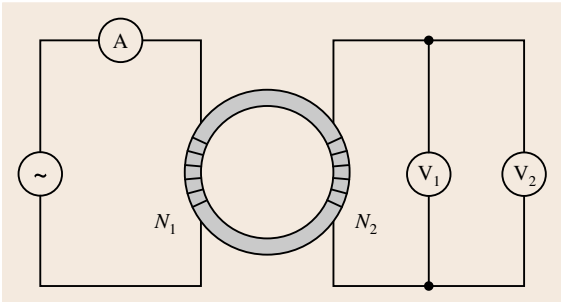

Fig. 10.21 Circuit diagram of the voltmeter–ammeter method. V_1 is an average-type voltmeter, V_2 is an rms voltmeter

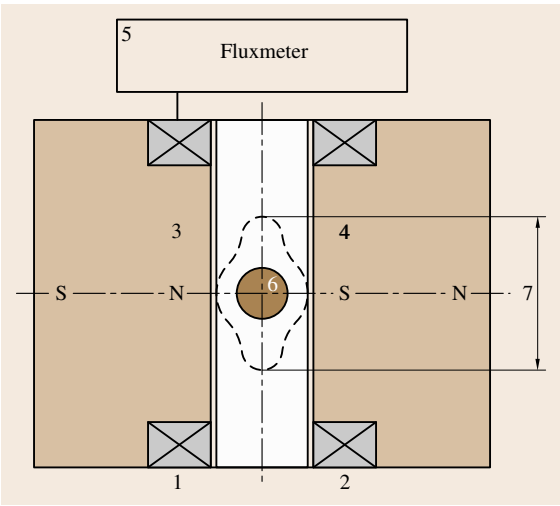

Fig. 10.22 Saturation coil: 1, 2 – windings of a Helmholtz coil, 3, 4 – permanent magnet material, 5 – fluxmeter, 6 – specimen; the *dashed line* (7) marks the maximum specimen volume for 1% accuracy

and the rms amplitude permeability from

$$\mu_{\mathrm{a,rms}} = \frac{\hat{B}}{\mu_0 \sqrt{2}\tilde{H}} , \qquad (10.27)$$

where $\tilde{H}$ is the rms value of the field strength.

Saturation Coil. The saturation coil, sometimes also called J_S-coil or saturation magnetometer, combines the moment-measuring coil with a permanent-magnet system that magnetizes soft magnetic specimens [10.16]. The measuring coil, usually a Helmholtz coil, is connected to a fluxmeter.

When a specimen with volume V is inserted into the coil, it is magnetized and the magnetic dipole moment j can be obtained from the flux measurement using (10.9). If the field strength is sufficiently high, the saturation polarization can be determined through

$$J_S = \frac{j}{V} . \qquad (10.28)$$

Of course the specimen can also be withdrawn from the coil for measurement, but the rotation method, which is frequently used with the moment-measuring coil, cannot be used.

For lower field strength the relative permeability can be calculated using

$$\mu_r = 1 + \frac{J}{H_i} . \qquad (10.29)$$

The inner field strength H_i of the specimen must be determined from the magnetizing field strength, taking into account the demagnetization factor.

The main applications of the method are the determination of the saturation polarization of specimens made of nickel or nickel alloys and the determination of the cobalt content in hard metal specimens.

Magnetic Scales. Magnetic scales or balances measure the force that acts on a magnetic specimen in a nonhomogeneous field [10.17]. From this force the following quantities can be determined

- magnetic moment m and magnetic dipole moment $j = \mu_0 m$,
- magnetic permeability μ and magnetic susceptibility $\chi = \mu - 1$.

As the specimens can be easily heated or cooled, the methods can also be used to measure the temperature dependencies of the properties. This includes the determination of Curie and Néel temperatures and the observation of other phase transitions.

Faraday Method. The force acting on a small specimen with volume V in a magnetic field with gradient $\mathrm{d}H/\mathrm{d}y$ is

$$F = j\frac{\mathrm{d}H}{\mathrm{d}y} = V\chi H\frac{\mathrm{d}H}{\mathrm{d}y} . \qquad (10.30)$$

The specimen is suspended from the scale so that it is located between the poles of an electromagnet (Fig. 10.23). The pole caps are shaped such that the product $H(\mathrm{d}H/\mathrm{d}y)$ is constant over the whole volume (gradient pole caps), so that the force is proportional to the susceptibility χ. The Faraday method is suitable for all kind materials, especially ferro- and ferrimagnetic specimens. It allows the determination of the saturation polarization J_S for soft magnetic materials if the specimen shape is appropriate.

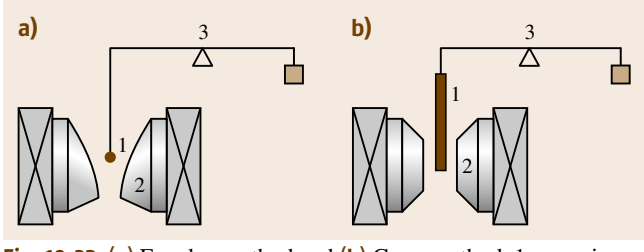

Fig. 10.23 **(a)** Faraday method and **(b)** Gouy method, 1 – specimen, 2 – electromagnet poles, 3 – balance

Gouy Method. A long bar-shaped specimen is suspended from the scale so that one end is located between the poles of an electromagnet generating a field strength H. The other end outside the poles is only affected by the stray field strength $H_s \ll H$. The force acting on the whole sample is

$$F = \tfrac{1}{2} A \chi \left(H^2 - H_s^2 \right) \approx \tfrac{1}{2} A \chi H^2 \,, \tag{10.31}$$

where A is the cross-sectional area of the specimen. The Gouy method is mainly used for para- and diamagnetic materials including liquids and gases.

Impedance Bridges. If an alternating current is supplied to a coil that contains a ferromagnetic core, a phase shift between magnetic field strength and flux density occurs. The magnetic material can be characterized by the complex permeability

$$\underline{\mu} = \mu' - \mathrm{i}\mu'' \,. \tag{10.32}$$

The impedance of the filled coil is

$$\underline{Z} = R + \mathrm{i}\omega L = \omega \mu'' L_0 + \mathrm{i}\omega \mu' L_0 \tag{10.33}$$

if losses and additional phase shifts that are not caused by the core material are neglected. L_0 is the inductance of the measuring winding without the magnetic core. For a cylindrical specimen, it can be calculated as

$$L_0 = \frac{\mu_0}{2\pi} \ln \left(\frac{D}{d} \right) h N^2 \,, \tag{10.34}$$

where D is the outer diameter, d is the inner diameter and h the height of the coil, and N is the number of turns of the winding.

The loss angle δ and the Q-factor can be determined from

$$\tan \delta = \frac{R}{\omega L} = \frac{1}{Q} = \frac{\mu''}{\mu'} \,. \tag{10.35}$$

For the determination of $\underline{Z}$, various impedance bridges are available from electrical measuring techniques; they differ in sensitivity and frequency range. For the characterization of magnetic components, suitable circuits are used in a frequency range of approximately 1 Hz to 100 MHz. A basic circuit is the Maxwell–Wien bridge shown in Fig. 10.24. It can be used from about 50 Hz to 100 kHz.

The specimen, a ring core that is uniformly wound with a single winding, is defined by its equivalent circuit diagram consisting of R_x and L_x. The bridge is balanced if

$$R_x = \frac{R_1 R_2}{R_v} \tag{10.36}$$

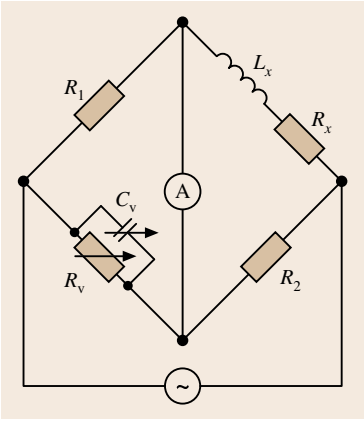

Fig. 10.24 Maxwell–Wien bridge

and

$$L_x = R_1 R_2 C_v \,. \tag{10.37}$$

R_x consists of the loss R caused by the magnetic core and the loss in the winding

$$R_x = R + R_0 \,. \tag{10.38}$$

The loss in the winding R_0 is basically the DC resistance if the frequency is not too high, and can be obtained from a resistance measurement.

The inductance L_x is composed of the leakage inductance L_σ and the inductance of the specimen L

$$L_x = L_\sigma + L = L_\sigma + \mu' L_0 \,. \tag{10.39}$$

For large permeabilities the leakage inductance L_σ can be neglected and μ' can be calculated to

$$\mu' = \frac{L}{L_0} \approx \frac{L_x}{L_0} \,. \tag{10.40}$$

Otherwise the real inductance L_0' of the winding should be considered. L_0' can be measured on an air-core coil: a winding that is wound on a nonmagnetic core and that has the same dimensions as the measuring winding. It can be assumed for small permeabilities that the stray field would be the same, regardless whether there is a core or not. With

$$L_0' \approx L_\sigma + L_0 \,, \tag{10.41}$$

it follows that

$$\mu' \approx 1 + \frac{L_x - L_0'}{L_0} \,. \tag{10.42}$$

At higher frequencies the resistance of the winding differs from the DC resistance due to the skin effect. In this case mutual inductance bridges provide more accurate results, as in these circuits the resistance of the wire does not enter the measuring result. The specimens must be equipped with two windings. Suitable circuits are the Wilde [10.18] and Hartshorn bridges. Further methods are compiled in [10.19].

Measurement of Magnetostriction. Magnetostriction comprises all dimensional changes of a specimen that are caused by changes in magnetization. For both the volume-invariant shape effect and the volume magnetostriction, a measurement of a change of the specimen length in one or more dimensions can be carried out.

The specimen is placed in the center of a solenoid, which generates the magnetic field required. The change in length is transferred via a rod to a displacement transducer that is located outside the stray field of the solenoid. The material of the rod must be properly chosen to keep the outer force acting on the specimen as small as possible and to avoid errors due to temperature-induced changes in length. Capacitive, inductive or optical sensors are used to measure the displacement.

Another method uses strain gauges that are directly attached to the specimen. To cancel out errors due to the magnetic and thermal properties of the strain-sensing element, a second element of the same type can be attached to a substrate that shows no magnetostriction but is exposed to the same environment. The two sensing elements can be connected to opposite paths of a bridge circuit.

A third method uses a single-mode optical fiber attached to the specimen. The fiber is part of an interferometer. The change in length is detected as a phase shift in the electromagnetic wave propagating in the fiber [10.20].

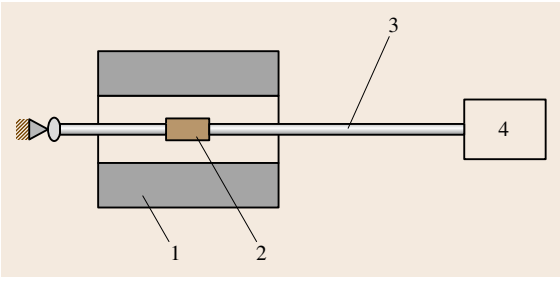

Fig. 10.25 Magnetostriction measurement: 1 – solenoid, 2 – specimen, 3 – specimen rod, 4 – displacement transducer

The volume magnetostriction can also be measured by the conventional measuring method for volumetric content. The specimen, immersed in a liquid, is exposed to the magnetic field.

Magnetostriction is an important parameter in many applications of electrical steel. A comprehensive description of magnetostriction measuring methods for these materials can be found in [10.21].

Measurement of the Hysteresis Loop of Amorphous or Nanocrystalline Ribbons

Sample Shape. In the case of soft magnetic ribbons the hysteresis loop can be measured on

1. open ribbons, in which case the demagnetizing factor has to be considered,
2. toroids.

The temperature the loop is measured is also important. In the case of low- or high-temperature measurements the system has to withstand the desired temperature.

In principle, magnetic measurements should always be carried out on a toroid instead of open ribbons because only then is a closed magnetic circuit realized. For ribbons this method has the disadvantage that the material is not in a stress-free state – there is a tensile stress on the outer surface and comprehensive stress on the inner surface. Another possibility is to use a single straight ribbon but then the demagnetizing field has to be considered.

Hysteresis Loop on a Single Ribbon. When hysteresis is measured on a single open ribbon a well-defined external stress can be applied. Temperature-dependent measurements are possible, although technically more complex. The facilities necessary for measuring the hysteresis loop are field coils, a compensated pickup coil, a current source, an ammeter and an integrator (fluxmeter). For the measurement of coercivity a Helmholtz coil is mainly used, and for the measurement of saturation magnetization the field is applied by a cylindrical coil producing a sufficient high field. The coils are energized by a computer-controlled power supply.

The devices are connected and controlled by a data-acquisition and control unit, forming a full automatic hysteresis-loop system. Figure 10.26 shows as an example a set up for such a hysteresis measurement on single strip ribbons.

In this case a compensated pickup system has to be used. When the pickup and the compensation coils are connected, so that the induction signals due to the field

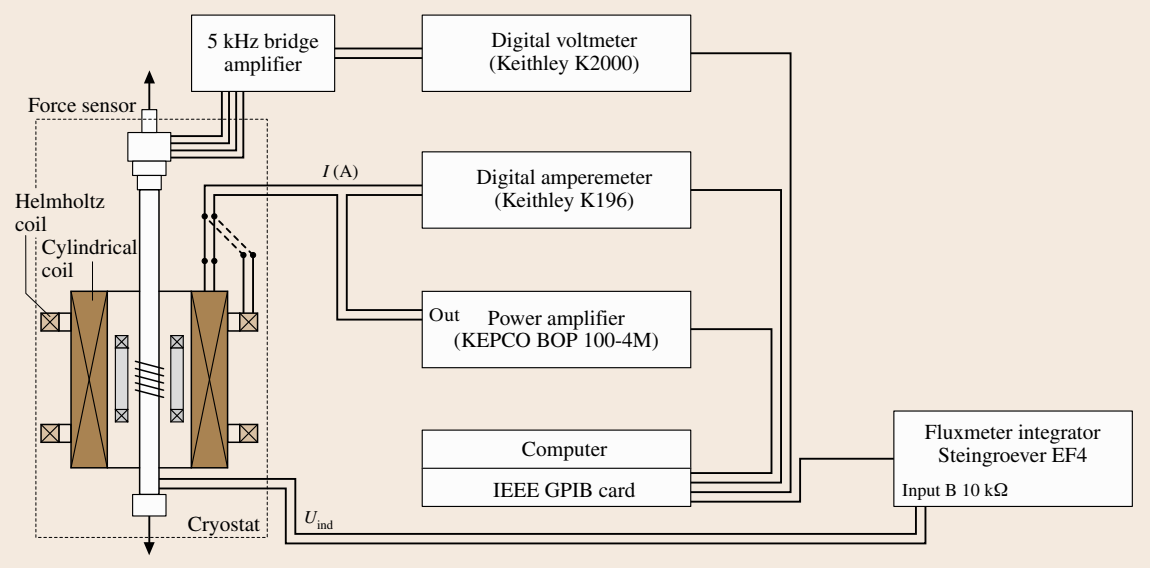

Fig. 10.26 Hysteresisgraph for a quasistatic hysteresis measurements and devices for force measurement for single ribbons

are subtracted, the remaining signal will be proportional to the magnetization M

$$u_{ind} = u_{pick} - u_{comp} = -N_{pick}\mu_0 A_{rib}\frac{dM}{dt} \ . \quad (10.43)$$

Magnetostriction. Magnetostriction on thin ribbons can be measured by direct and indirect methods. Direct methods are, for example, measurements with strain gauges, capacitance transducers or interferometers. All these methods have the disadvantage that sample preparation is difficult. Strain gauges are limited in sensitivity ($\Delta\lambda/\lambda_0 = \pm 1 \times 10^{-6}$) . Additionally the saturation magnetostriction constant has to be determined from measurements parallel and perpendicular to the external field.

Indirect methods are the Becker–Kersten method [10.22] and the small-angle magnetization-rotation (SAMR) method [10.23]. With the Becker–Kersten method the magnetostriction is determined from the stress dependence of the hysteresis loop. The SAMR method was developed by Narita et al., especially for ribbon shaped materials with a small magnetostriction constant.

The SAMR Method. First of all a DC field is applied in the ribbon axis. This field should magnetically saturate the sample. Then a smaller AC field (with frequency f) is applied perpendicular to the ribbon axis. This causes a small rotation (small angle) of the magnetization vector out of the ribbon axis. A small induction signal with double the frequency of the AC field is now detected by a pickup coil (Fig. 10.27a) and measured by a lock-in amplifier. Applying an external stress to the ribbon causes, for ribbons with positive magnetostriction, a decrease in the deflection angle, whereas for samples with negative magnetostriction the angle increases (Fig. 10.27b). Now the DC field H_{DC} is changed in such a way that the deflection angle and therefore

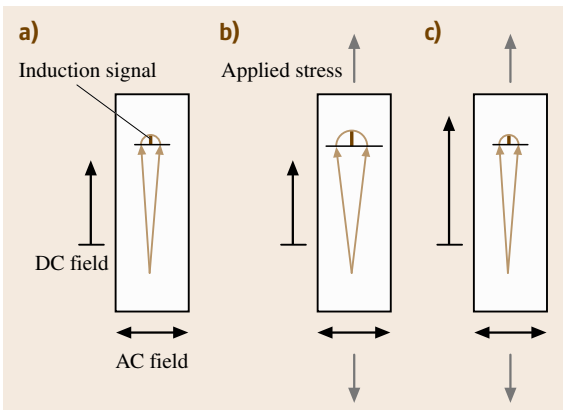

Fig. 10.27a–c Magnetostriction measurement by the SAMR method

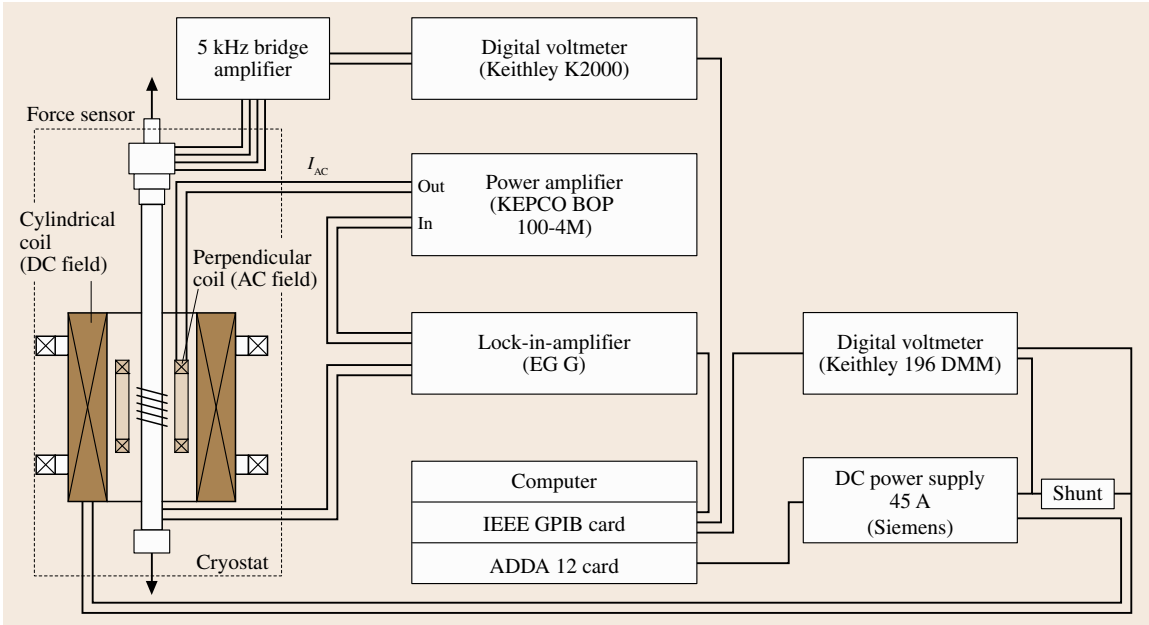

Fig. 10.28 Experimental set up for magnetostriction measurement by SAMR method

also the induction signal go back to their initial value (Fig. 10.27c). The variation of the DC field ΔH_{DC} and the variation of the external stress $\Delta\sigma$ determine the magnetostriction constant. To get an accurate value this procedure has to be repeated step by step with increasing stress. From the balance of the magnetic and the magnetoelastic energy one can calculate the saturation magnetostriction as

$$\lambda_s = -\frac{1}{3} J_s \left(\frac{\Delta H_{DC}}{\Delta\sigma}\right)\Big|_f = -\frac{1}{3}\frac{\Phi_{sat}}{A_{rib}}\left(\frac{\Delta H_{DC}}{\Delta F/A_{rib}}\right) = -\frac{1}{3}\Phi_{sat}\left(\frac{\Delta H_{DC}}{\Delta F}\right), \quad (10.44)$$

where J_s is the saturation polarization of the ribbon at a certain temperature. The polarization J_s is proportional to α/A_{rib}, where α is the output value of the fluxmeter and A_{rib} is the cross section of the sample. The value of $\Delta\sigma$ is given by $\Delta F/A_{rib}$. According to the equation above the magnetostriction then becomes completely independent of the cross section. The magnetostriction then depends only on the exact measurement of the magnetic flux (saturation value Φ_{sat}), on the measurement of the force $F(\Delta F = F_1 - F_2$, by the force-sensor bridge) and on the measurement of the magnetic field H_{DC} ($\Delta H_{DC} = H_{DC_1} - H_{DC_2}$). Figure 10.28 shows as an example a possible set up for magnetostriction measurements using the SAMR method.

This method was used successfully to determine the magnetostriction of many amorphous materials [10.24]. It delivers comparable results and achieves a sensitivity in the magnetostriction constant of up to 10^{-9} [10.25].

Magnetoimpedance. Relevant information about transversal magnetization processes in magnetic materials can be obtained from the field H and frequency f dependence of the complex impedance ($Z = R + iX$). In soft magnetic high-permeability materials, large variations of Z (for current frequencies larger than 100 kHz) have been observed upon the application of relatively small magnetic fields, the so-called giant magnetoimpedance effect (GMI) [10.26–28]. Generally magnetoimpedance is based on the application of an AC field caused by an inhomogeneous field distribution in a conducting material with a high permeability. This effects depends therefore on the frequency, and on the applied field, but also on material parameters such as the conductivity as well as the permeability – which depends additionally on the applied DC field – of the material. Additionally the sample geometry (ribbons, wires) as well as local fluctuations of material parameters have to be considered.

For these measurements one needs: a digital lock-in amplifier working over a broad frequency range, a power supply, a dynamic signal analyzer, some form of digital multimeter, and a computer with an interface for the data acquisition. The lock-in amplifier supplies the AC signal and is also employed to read the real and imaginary voltage drop across the sample. In GMI measurements, a constant-current source supplies a constant AC current flowing along the sample in order to assure a constant circular magnetic field. As the generator of the lock-in works generally as a constant-voltage source, either one uses an external constant-current source or one measures the AC voltage drop across a resistor R, which determines the actual current through the sample as shown in Fig. 10.4. In this experiment not only the AC current has to be controlled but also the phase signal. In order to do this a two-position relay controlled by a computer can be used; the two positions correspond to calibration and measurement. In the calibration position (Fig. 10.29), the signal is applied to the sample, which is in series with a grounded resistor and the lock-in measures the voltage across the resistor, which can be controlled to maintain a constant intensity value. In the measurement position (Fig. 10.29), the relay inverts the ground and signal position so that the signal is applied to the resistor, and the sample is grounded. The lock-in thus measures the sample's signal. The voltage over the sample is measured in a four-probe configuration and the contacts with the sample are made using silver conducting ink.

The magnetic DC field, which is applied along the sample's length, is supplied by a pair of Helmholtz coils connected to a power supply, which operates as a current source. The current passing through the coils is measured by a multimeter. With this equipment the magnetoimpedance as a function of frequency and external DC field can be measured. Furthermore, the experimental set up can be completed by a dynamic signal analyzer, which allows one to follow the time dependence of the impedance after a sudden rearrangement of the domain configuration [10.29]. After the magnetic field is switched off ($t = 0$), it is possible to measure both R and X from t_0 up to t_1 by connecting the DC output of the lock-in to one of the inputs of the signal analyzer. The sensitivity is high enough to notice relative variations as low as 0.1%. With this extension magnetic disaccommodation of the magnetoimpedance can also be measured.

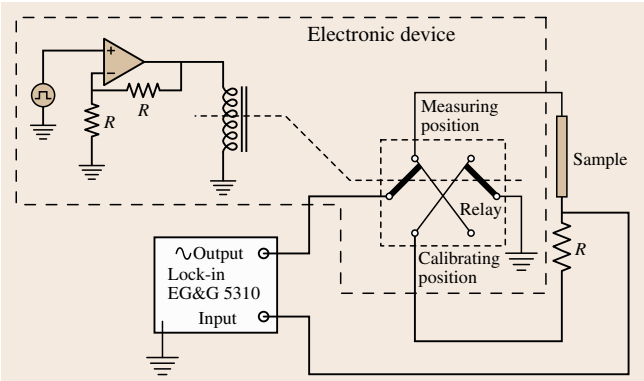

Fig. 10.29 Schematic diagram of the electric necessary to measure the magneto-impedance

10.3 Magnetic Characterization in a Pulsed Field Magnetometer (PFM)

Industrial producers and consumers of magnets are increasingly demanding systems which allow fast and reliable online tests of the hysteresis properties of magnets. High-quality permanent magnets based on rare-earth intermetallic compounds such as Sm-Co and Nd-Fe-B exhibit coercivities of 2 T and sometimes even higher, which are too high for Fe-yoke-based systems [10.7, 30].

The current conventional methods, namely vibrating-sample magnetometers (VSMs) and permeameters have limiting physical constraints. Fe-yoke-based VSMs and permeameters offer only a limited field strength (maximum 1.5 T). Permeameters are used for measuring the second quadrant of the hysteresis loop and need careful sample preparation (cutting, polishing). VSMs that use a superconducting solenoid require liquid helium for cooling and are generally expensive; additionally standard magnetometers are currently only available for relatively small samples (mm sizes). Additionally superconducting solenoids allow only limited field-sweep rates ($\mathrm{d}H/\mathrm{d}t$ rates) which are of the order of T/min. Generally all these systems need special sample preparation and measurement times that are unacceptable for industrial purposes. It will be shown that a PFM is

a new instrument that is well suited for fast and reliable measurement of the hysteresis loops of hard magnetic materials.

10.3.1 Industrial Pulsed Field Magnetometer

A short-pulse system (typical pulse duration 1–50 ms) has a condenser battery as an energy source, which has a certain size given in kJ (typical values are 10–100 kJ). The available power determines the time constant of the total system.

Figure 10.30 shows a block diagram of a pulsed field magnetometer (PFM) [10.10, 31]. A pulsed field magnetometer consists of

1. the energy source, generally a capacitor battery; the stored energy is given by $CU^2/2$. The maximum charging voltage can be 1–30 kV. The capacitance determines the costs of such a system, the maximum sample size and the time constant. For a magnetometer that can measure the full loop, voltage reversal on the battery must be allowed.
2. charging unit, which should generate a reproducible and selectable charging voltage; it determines the repeatability of the achieved field in the pulse magnet.
3. pulse magnet: for an existing energy, the pulse magnet determines, via its inductivity, the pulse duration. Additionally the volume (diameter, homogeneity) limits the dimensions of the experiment inside of the magnet. Heating during a pulse may be also a problem when high repetition rates are desired.

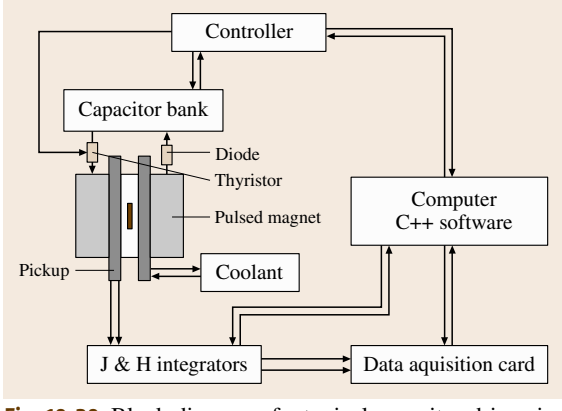

Fig. 10.30 Block diagram of a typical capacitor-driven industrial PFM

4. measuring device: this consist of the pickup system and the measuring electronics (amplifiers, integrators, PCs, data storage). A careful design of the pickup system is very important in order to achieve a high degree of compensation and consequently a good sensitivity.
5. electronics: this consist either of a digital measuring card or of a storage oscilloscope which is connected to a modern data-acquisition system on a standard PC, which allows a software-supported operation of the PFM (charging, discharging and the measurement with an evaluation of the resulting loop). In order to obtain a reasonable accuracy the analog-to-digital converters (ADCs) of the storage oscilloscope (measuring card) should have a resolution of at least 12 bit.

High-Field Magnets

The pulse magnet has to be optimized with respect to the available power, the heating of the magnet and the stresses. The field homogeneity over the desired length of the experiment should be better than 1%. In systems where the hysteresis loop is measured, the pulse magnet has to be optimized with respect to low damping and also for a certain measuring task (maximum field, pulse duration, pulse shape, sample volume).

Pickup Systems

Generally the magnetization is measured using a pickup coil system, which has to be compensated in order to measure the magnetization M instead of the induction B. For this purpose different arrangements of pickup coils have been developed (Fig. 10.31). It was found that a coaxial system based on Maxwell coils is best suited to this purpose [10.32]. The main idea of constructing a pickup system is that the space distribution of the field around the sample is first developed into a dipole (and quadruple) contribution. These contributions should be compensated in order to cancel the effect of the external field. Therefore such systems consist of at least two coils (Fig. 10.31c). The induced voltages can be written as

$$u_1(t) = -\mu_0 N_1 K_1 \left(R_1^2 \pi\right) \left(\frac{\mathrm{d}H}{\mathrm{d}t} + \frac{\mathrm{d}M}{\mathrm{d}t}\right) ,$$

$$u_2(t) = -\mu_0 N_2 K_2 \left(R_2^2 \pi\right) \left(\frac{\mathrm{d}H}{\mathrm{d}t}\right) ; \qquad (10.45)$$

where u_i, N_i, $K_i R_i$ $(i = 1, 2)$ are the induction voltage, number of windings, coupling factor, radius of the outer $(i = 1)$ and inner $(i = 2)$ pickup coil, respectively.

Dipole compensation is fulfilled when $R_1^2 N_1 = R_2^2 N_2$ is valid. The coupling factor with respect to the field H is the same for both coils, but not with respect to the sample. It is assumed that for the outer coil the voltage due to the magnetization can be neglected (in reality there exists a small induction voltage due to M which only reduces the calibration factor). Subtracting now the signal of the two antiparallel-wound coils causes a cancelling of the effect of the field, which yields the dipole compensation. Also higher multipoles can be compensated, which leads to a more complex pickup system for which more space is necessary. Therefore for pulsed field systems usually only the dipole compensation is used.

For some applications the pickup system should be cooled in order to hold a stable temperature, which is especially important for a room-temperature system with a high repetition rate. The details of such a pickup system as well as electronic balancing are described in [10.33].

For an industrial system a reasonable sample size is important; typical values are samples up to 30 mm in diameter and 10 mm in length within a ±1% pickup homogeneity range. For magnetic measurements exact positioning (reproducibility better than 0.1 mm) in the PFM is necessary.

10.3.2 Errors in a PFM

The Demagnetizing Factor

In a magnetically open circuit the correction for the demagnetizing factor N is a very important step to get the true hysteresis loop as a function of the internal field H_{int}. For ellipsoids and spheres the demagnetizing field H_{d} is simply written

$$H_{\text{int}} = H_{\text{ext}} - NM\,,$$
$$H_{\text{d}} = NM\,. \qquad (10.46)$$

The demagnetizing factor N is just a number $0 < N < 1$ for a sphere ($N = 1/3$) or an ellipsoid. In all other cases the demagnetizing field H_{d} is no longer constant.

Important points such as the remanence and the working point, but also the energy product $(BH)_{\text{max}}$, depend strongly on N. Unfortunately in industry more complex shapes, such as cylinders, cylinders with holes and even arc segments, are used. In this case N can become a tensor according to the symmetry of the sample. For complex shapes a finite-element package has to be used in order to calculate the stray field.

In order to investigate the effect of N for simple shapes in Fig. 10.32 the demagnetizing curves in the second quadrant for an anisotropic ferrite HF 24/16 are drawn. The two samples were from the same batch, one was a cylinder and one a sphere. The shape of the loops agrees very well. This means that in this special case the use of a constant number for N even for the cylinder is sufficient for the correction.

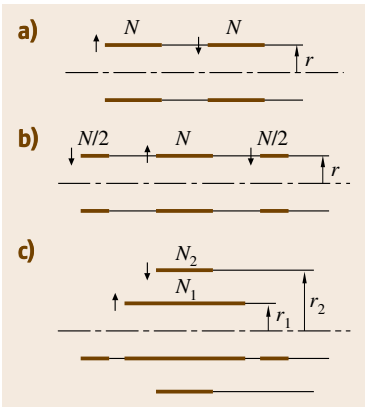

Fig. 10.31a–c Scheme of a coaxial pickup system for measuring the magnetization

Figure 10.33 shows the hysteresis loop as measured on a cylindrical sample with a hole (outer diameter 19 mm, hole: 3.17 mm; $h = 2$ mm) of plastic-bonded Nd-Fe-B-type material. Assuming $N = 0.45$ gives a remanence of 0.666 T, whereas assuming $N = 0.55$ delivers a remanence of 0.682 T. The static value measured with an electromagnet was 0.682 T. This demonstrates the problem of such an unknown demagnetizing factor. It is impossible to say what the correct value is really.

Finally it should be mentioned that the problem discussed here of an unknown demagnetizing factor is not only a problem for the PFM; this is a general problem

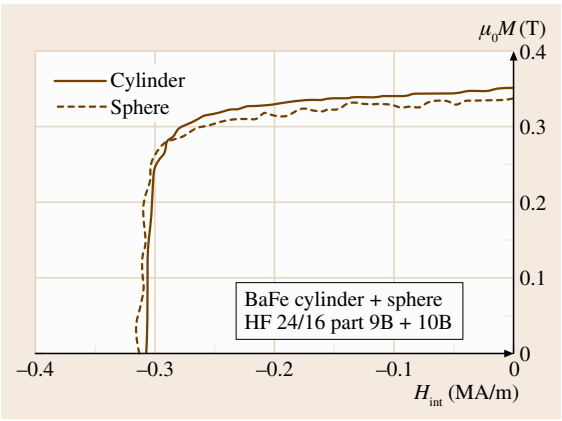

Fig. 10.32 Demagnetizing curve as obtained for a spherical and a cylindrical anisotropic Ba-ferrite (HF 24/16)

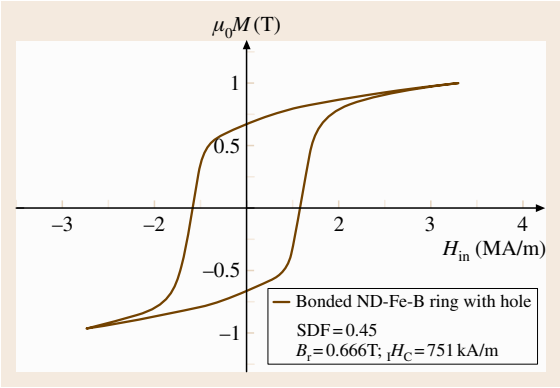

Fig. 10.33 Hysteresis loop of a cylindrical sample with a hole of plastic-bonded Nd-Fe-B-type material

for all magnetometers using a magnetically open circuit, such as e.g. in a VSM or also in a SQUID.

Transient-Field Errors

The application of transient fields causes errors, which have to be considered. Two possible errors may arise in pulsed field measurements due to the field sweep rate $\mathrm{d}H/\mathrm{d}t$

a) Eddy current errors,
b) Magnetic viscosity effects.

Eddy Currents and Their Solution [10.34]

A time-dependent external magnetic field in a metallic conducting sample causes, according to Maxwell equations, currents (*eddy currents*), which create a dynamic magnetic moment that is antiparallel to the external field, as is demonstrated in Fig. 10.34. The time behavior is exponential: $I(t) = I_{0\mathrm{eddy}} \exp(-r/M)t$, where M is a dynamic mutual inductance and r is also a differential resistance due to the path of the eddy currents.

It can be shown [10.34] by solving the Maxwell equations for an electrical conducting material (without considering the permeability) that the dynamic magnetization due to eddy currents can be written as

$$\boldsymbol{M} = \mathrm{curl}\boldsymbol{j} = -\sigma \frac{\partial}{\partial t}(\mathrm{curl}\boldsymbol{A}) = \sigma \frac{\partial \boldsymbol{B}}{\partial t} = \frac{\mu}{\rho}\frac{\partial \boldsymbol{H}}{\partial t} \,. \tag{10.47}$$

This means that plotting the magnetization m due to eddy currents versus $\mathrm{d}H/\mathrm{d}t$ of a conducting sample delivers a linear relation where the slope is proportional to σ (specific electrical conductivity) which is equal to $1/\rho$ (specific electrical resistivity), as is also found experimentally.

The maximum eddy-current density ($J_{\max} = J(r_{\mathrm{sample}}, z = 0)$) of all samples with different pulse duration and their magnetic moment m_{FEMM}, m_{FEMM} can also be calculated using a finite element package such as FEMM by *Meeker* [10.35] (2-D finite-element software). For samples that are not large and frequencies that are not high a linear relation between the eddy-current density and the radius r holds, which gives a rather simple solutions for calculating the dynamic eddy-current magnetization, as follows.

The magnetization for a cylinder is

$$M = \frac{j_{\max} r_{\mathrm{s}}}{4} \,. \tag{10.48}$$

Hence, the magnetization is independent of the height of the cylinder.

A similar calculation delivers the magnetization for a sphere

$$M = \frac{j_{\max} r_{\mathrm{s}}}{5} \,. \tag{10.49}$$

To prove the assumption that the magnetization due to the eddy-current density increases linear with the radius but stays constant with the height of the sample, several cylindrical and spherical samples of Cu were studied [10.34]. It was demonstrated that the measured maximum magnetization can be fitted with a function $f = Cr^2$, where r is the radius of the sample, which gives, as theoretically expected, a quadratic dependence as shown in Fig. 10.35.

On the experimental side, in agreement with the formulas above, the eddy currents were found to be independent of the height of the sample [10.36].

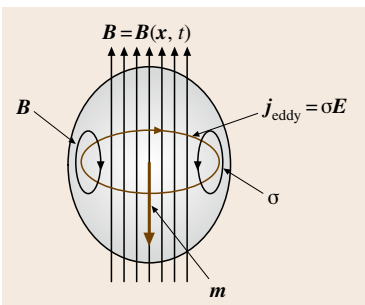

Fig. 10.34 The principle of eddy currents in a metallic sample

Conducting, Magnetic Samples – *f*/2*f* Method [10.37, 38]

In a magnetic material the eddy currents are determined by the electrical conductivity σ but also by the perme-

ability μ, where the latter is also a nonlinear function of the external field. In this case the eddy-current problem cannot be solved analytically. Here, numerical methods are the only possible way. However in some cases simplifications are possible. In order to correct the hysteresis loop of a hard magnetic material as measured in a PFM for the eddy-current error a special method was developed. The hysteresis loop of each sample is measured with two different pulse durations, f and $2f$, which generate the same J signal with respect to the applied field but with the addition of different dynamic magnetizations due to eddy-current distributions. The eddy currents are related to the frequency; the eddy-current magnetization is approximately proportional to $\mathrm{d}H/\mathrm{d}t$, as was shown already. By processing the two measurements it is possible to remove the error due to eddy currents, producing the direct equivalent of a static hysteresis plot; this approach is known as the $f/2f$ method [10.37, 38]. This method is based on the following equations

$$H_\mathrm{m} = H_\mathrm{ext} - H_\mathrm{eddy} + H_\mathrm{d}\,, \tag{10.50}$$

where H_ext is the external field applied by the pulse, H_eddy is the dynamic field caused by the eddy currents, and H_d is the demagnetizing field.

The polarization J appearing in a pulse-field experiment consists of two components, the true polarization $J_\mathrm{DC}(H_\mathrm{DC})$ as measured as a function of a DC field H_DC and the apparent polarization due to eddy currents J_eddy. Now performing two experiments, one with a short pulse (described by "s") and one with a long pulse (described by "l") one gets a set of field data and polarization data

$$H_\mathrm{ext,s} + \frac{J_\mathrm{eddy,s}}{\mu_0} = H_\mathrm{ext,l} + \frac{J_\mathrm{eddy,l}}{\mu_0}\,. \tag{10.51}$$

Based on these equations a mathematical procedure was developed which delivers the so-called $f/2f$ correction. This method can be applied under the general assumption of a sufficiently small eddy-current error, which means less than 20%. The validity and the limits of the $f/2f$ method were investigated and proofed by a three-dimensional (3-D) finite-element calculation [10.39]. Therefore, this so-called $f/2f$ method seems to be a good way to correct eddy-current errors in the measured hysteresis loop.

Application of the $f/2f$ Correction to a Magnet

To test the $f/2f$ correction a large cylindrical commercial Nd-Fe-B magnet from VAC (Vacodym 510, Charge 210105) was measured (Fig. 10.36). This cylinder had a diameter of $d = 20\,\mathrm{mm}$, and a height of 6.9 mm. The static data measured by VAC were: remanence $B_\mathrm{R} = 1.296\,\mathrm{T}$, and coercivity ${}_\mathrm{I}H_\mathrm{C} = 1255\,\mathrm{kA/m}$.

The $f/2f$-corrected coercivity value was found to be 1275 kA/m, which is 2% too high. The measured remanence value of 1.25 T is about 2% too low. This is experimental proof of the validity of this $f/2f$ correction.

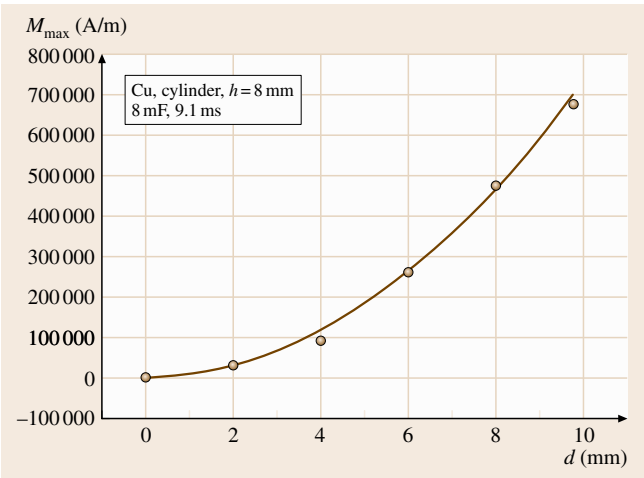

Fig. 10.35 Dependence of the maximum eddy-current magnetization on the radius

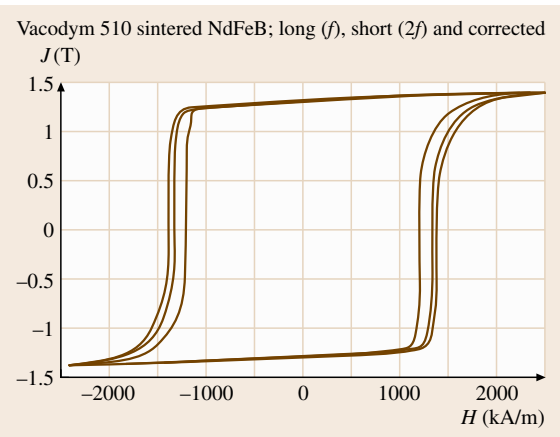

Fig. 10.36 Room-temperature hysteresis loop as obtained on a large (20 mm diameter) sintered Vacodym 510 magnet. One loop was measured with a long pulse (time duration of 57 ms) and one with a short pulse (time duration of 40 ms) (*outer loop*). The *inner lying* loop represents the corrected hysteresis

Magnetic Viscosity

The magnetic viscosity can influence the shape of a in a PFM-measured hysteresis loop. This leads especially to higher coercivity values measured in a transient field. The general questions are: how large is this error, when is this error not negligible, what is the origin of this error, and can this error be corrected?

The effect of magnetic viscosity has been well known for many years and has been investigated for many hard magnetic materials [10.40, 41]. It has also been shown that the magnetic viscosity coefficient S_v can be used to determine the activation volume, an important parameter for the understanding of the coercivity mechanism [10.42]. The viscosity coefficient is usually determined by static field measurement. One measures the loop $M(H)$ and stops in the second quadrant with this measurement at a certain field H. There under the condition $H = \text{const.}$ the time dependence of M is measured, from which the magnetic relaxation coefficient $S = \mathrm{d}M/\mathrm{d}\ln t$ can be determined. For calculating S_v one needs also the irreversible susceptibility χ_{irr}. One has to consider that the typical field sweep rate in pulsed field experiments $\mathrm{d}H/\mathrm{d}t$ is approximately 1000 T/s, which is 10^6 orders of magnitude larger than the field sweep rate $\mathrm{d}H/\mathrm{d}t$ that can usually be achieved in VSMs using an electromagnet or a superconducting coil. Generally, the viscosity coefficient (S_v) determined from static field measurements (denoted by S_{vJ}) is much smaller than that obtained from PFM measurements (denoted as S_{vp}). However, it may be of great importance that the time windows in these two experiments are completely different.

Experimental Method to Determine Viscosity

In order to obtain the coercive field of the specimen under fields with different sweep rates, hysteresis loops of the samples are recorded at a fixed temperature by using a pulse field magnetometer (PFM) applying a sufficiently high maximum field. The sweep rate $\mathrm{d}H/\mathrm{d}t$ can be changed either by varying the capacitance of the condenser battery or by changing the amplitude of the field or both; with this method field sweep ranges from about 0.5 up to 20 GA $\mathrm{m}^{-1}\mathrm{s}^{-1}$ and even higher are possible. The dependence of the coercivity on the field sweep rate $\mathrm{d}H/\mathrm{d}t$ can be used to estimate the viscosity S_v (10.52)

$$S_{vp} = \frac{H_{C_1} - H_{C_2}}{\ln\left[(\mathrm{d}H_1/\mathrm{d}t)\,/\,(\mathrm{d}H_2/\mathrm{d}t)\right]}\,. \qquad (10.52)$$

This method and its limitation were recently demonstrated on the model material $SmCo_{5-x}Cu_x$ and related compounds [10.43].

The Magnetic Viscosity in $SmCo_{5-x}Cu_x$ Alloys [10.43]

$SmCo_5$ is nowadays a standard permanent-magnet material. However, substituting Co by Cu causes a change of the coercivity mechanism from nucleation to pinning. Additionally it was found that in $Sm(Co, Cu)_5$ a large magnetic-viscosity effect appears. Therefore this is also a model material in order to investigate viscosity effects in a PFM. In Fig. 10.37 the coercive field as a function of $\mathrm{d}H/\mathrm{d}t$, as measured in as-cast and annealed $SmCo_{5-x}Cu_x$ magnets, is presented. The coercivity increases with $\mathrm{d}H/\mathrm{d}t$, providing evidence for the existence of a strong magnetic aftereffect.

Conclusion

a) Eddy-current errors. The application of a transient field causes eddy currents in metallic samples which lead to a dynamic magnetization M_{eddy} that is proportional to $\mathrm{d}H/\mathrm{d}t$ [10.34]; the proportionality factor is the specific electrical conductivity. Additionally, M_{eddy} scales with R^2 (R is the radius of a rotational symmetrical sample), which means that the error increases quadratically with increasing sample diameter [10.34]. Fortunately most of the metallic permanent magnets are sintered materials where the specific resistivity (typically $2\times10^{-4}\ \Omega\,\mathrm{m}$) is generally a factor 50–100 higher

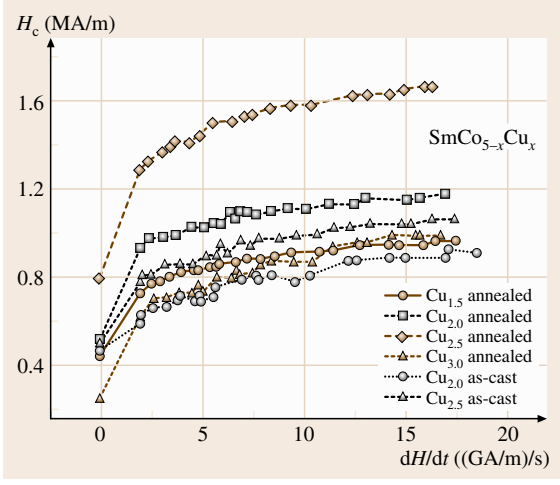

Fig. 10.37 Coercive field as a function of the sweep rate $\mathrm{d}H/\mathrm{d}t$ measured in as-cast and annealed $SmCo_{5-x}Cu_x$ alloys

that of Cu. Therefore the error in magnetization measurements due to eddy currents is rather small. These considerations have led to the development of eddy-current correction for hysteresis loops measured in pulsed fields, which is called the $f/2f$ method. In this case one measures the loop with two different pulse durations and calculates the corrected loop point by point, applying an extrapolation procedure [10.37, 38]. It was shown by finite-element calculations that for eddy-current errors that were not too large (less than 20%) the corrected loop agrees with the true loop within 2%. This means that the effect of eddy currents is understood and can be corrected in most cases [10.39].

b) Magnetic viscosity effects. When the hysteresis loop of hard magnetic materials is measured in transient fields the so-called magnetic viscosity causes a difference between the measured loop and the true loop. The magnetic viscosity is also observed in nonconducting materials (e.g., ferrites), therefore it is not due to eddy currents. It has to be mentioned that the time constant of the exponential decay of of eddy currents (in metallic samples) is of the order of typical values of microseconds, whereas that of the logarithmic decay of the viscosity lies between milliseconds and seconds. Additionally eddy currents depend on the geometry of the sample whereas this is not the case for the viscosity.

10.3.3 Calibration [10.1]

Field Calibration

The field is calibrated using a small pickup coil whose effective winding area is known from an NMR calibration. The induced voltage $u(t)$ is then fitted using (10.53), in order to determine the field calibration factor k, the damping factor and the pulse duration (including the effect of the damping)

$$\begin{aligned} H &= H_0 \exp(-at) \sin \omega t \,, \\ u_i(t) &= -\mathrm{NA} \frac{\mathrm{d}B}{\mathrm{d}t} \\ &= -\mathrm{NA}\mu_0 H_0 \frac{\mathrm{d}}{\mathrm{d}t} \left[\exp(-at) \sin \omega t\right] \,. \end{aligned} \tag{10.53}$$

The damping factor a determined in this way can be compared with the value given by a PFM circuit using $a \approx R/2L$ (where R is the resistivity of the pulse magnet, and L is the inductivity of the pulse magnet).

The calibration factor k is also determined as a function of the gain (integrator gain and the gain of preamplifier). The calibration factor k gives a relation between the induced voltage and the field at the search coil. At the same time the integrated voltage (using different gain factors) of the H-measuring coil (which is located at the pickup rod) on the magnetometer system is recorded.

It was shown that the calibration factor k was also determined as a function of the gain using an analogue integrator [10.1]. The scattering of the k factor was below $\pm 1\%$. This indicates that the linearity of the gain is better than 1%. Using such a procedure, an absolute field calibration of better than 1% is achieved, including the time constants (gain) of the integrator.

Magnetization Calibration

The magnetization is calibrated using well-known materials such as Fe and Ni (in which the eddy-current error causes an uncertainty) or preferably a nonconducting sample such as Fe_3O_4 or a soft magnetic ferrite, such as 3C30 (Philips). All calibration measurements are performed at room temperature. The results of the magnetization calibration measurements are summarized in Table 10.3. To check the reproducibility all measurements were repeated 10 times to give an average value $\langle M \rangle$. Additionally measurements using a shorter pulse duration (40 ms) were performed, which were generally in good agreement with that of the long pulse. For the metallic samples an error of 1–2% due to the eddy currents occurs.

The mean value of the deviations $D_{\mathrm{mv}} = 1.6\%$ is higher than the true values. It should be mentioned that no significant differences in the measured magnetization values were obtained, when different pulse duration were employed.

The mean value of the deviations $D_{\mathrm{mv}} = 1.6\%$ has a standard deviation of 0.95%. The standard deviations concerning the reproducibility gave a mean value of

Table 10.3 Summary of calibration results

Sample	Shape	$\mu_0 H_{\max}$ (T) $t = 57$ ms	$\langle \mu_0 M \rangle$ (T)	$\mu_0 M_{\mathrm{literature}}$ (T)	Error (%)	$\mu_0 M$ (T) $t = 40$ ms
Fe_3O_4	Sphere $2r = 5.5$ mm	1.5	0.5787 ± 0.001	0.569 [10]	+1.6	0.5782
Ni	Cylinder $D = 4$; $h = 8$ mm	1.5	0.6259 ± 0.0008	0.610 [11]	+2.6	0.6322
Fe	Cylinder $D = 4$; $h = 8$ mm	4.5	2.1525 ± 0.0051	2.138 [12]	+1.4	2.1826

0.19%. Therefore, the deviation is, in the worst case, 1.14%. This means that the magnetization value could be calibrated with an absolute accurately of ±1.14%.

Reliability of Calibration

For testing the reliability of the calibration procedure a *calibrated sample* from the Physikalisch-Technische Bundesanstalt (PTB) in Braunschweig, Germany was measured. This sample was an anisotropic barium-ferrite from Magnetfabrik Schramberg with a cylindrical shape, with a height of 10 mm and a diameter of 6 mm. The mass was 1.417 g. The hysteresis measurement was performed by applying an external field of 2 T and a pulse duration of 56 ms. In order to reduce the statistical error the measurement was repeated 7 times.

The mean value of the remanence magnetization determined in this way is $B_r = (0.3644 \pm 0.0002)$T, which corresponds to an error of ±0.05%. PTB gave a remanence value of $B_r = (0.3625 \pm 0.0044)$T. So the difference between the PFM and the PTB value is about 0.5%, which is smaller than the given calibration error.

In order to test the effect of pulse duration, the PTB-calibrated sample was measured under the same conditions but with different pulse durations (56 ms and 40 ms) (Fig. 10.38). The difference in the remanence magnetization is below 1%. It should be noted that also the measured coercivity is only 2% higher, than the PTB value, which strongly supports the reliability of our field calibration.

Table 10.4 Summary of calibration measurement

Sample	$\mu_0 M_{meas}$ (T)	S (%)	$\mu_0 M_{literature}$ (T)	Deviation (%)
Fe_3O_4	0.5787	0.2	0.569	+1.6
Nickel	0.6259	0.13	0.610	+2.6
Iron	2.1525	0.24	2.138	+0.7

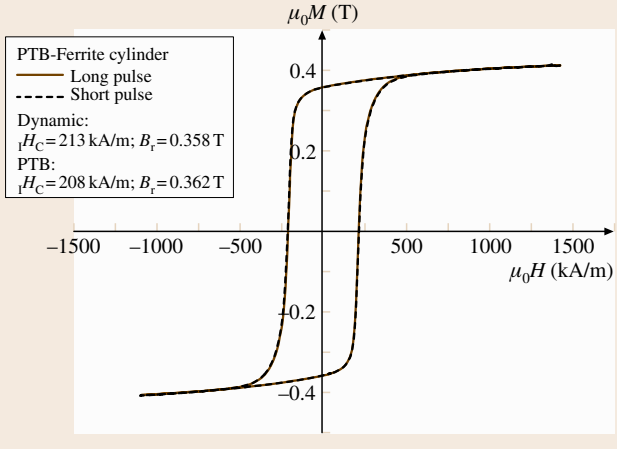

Fig. 10.38 Comparison of the on the PTB-magnet measured magnetization for a short and long pulse

Influence of Sample Geometry on Magnetization Values

In order to investigate the effect of the sample geometry on the accuracy of the magnetization measurements in the PFM, a set of industrial soft magnetic ferrites with different shapes were used (Philips (3C30)). All samples were from one batch. This material has a magnetization at room temperature of about 0.55 T, whilst the Curie temperature was about 240 °C. The density is 4800 kg/m^3. Since this material is an insulator, there are no eddy-current effects. The chosen shapes are given in Table 10.5.

The samples were measured in an external field with an amplitude of 2 T and a pulse duration of 56 ms. All samples were measured at room temperature (21 °C ± 1 °C) using the same amplification factor and the same mechanical adjustments. Small deviations are visible in the shape of the hysteresis loops, especially where the saturation enters the high-permeability region (Fig. 10.39). This is due to the fact that the mean

Table 10.5 Shapes and masses of the 3C30 samples

Sample (mm)	Size	Mass (g)
Sphere	$d = 9.1$	$m = 1.9065$
Small cube	11.2 × 11 × 0.8	$m = 0.5226$
Medium cube	11.9 × 11.9 × 3	$m = 1.9316$
Big cube	21 × 14.6 × 11.9	$m = 17.3848$

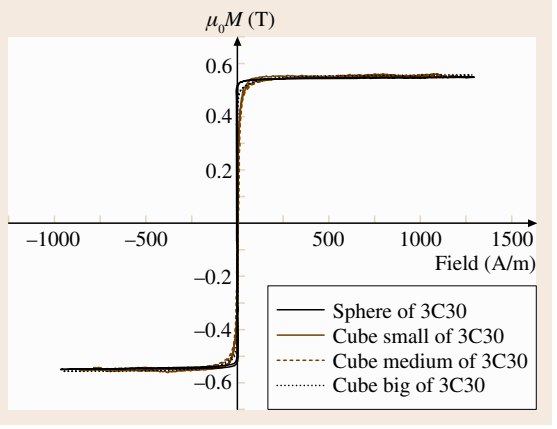

Fig. 10.39 Hysteresis measurements on 3C30 samples with different shapes

Table 10.6 Magnetization at $H = 2\,\mathrm{T}$ of 3C30 samples

Sample	Magnetization (T)
Sphere	0.550
Small cube	0.558
Medium cube	0.555
Big cube	0.557

demagnetization factor causes an error, which becomes especially significant in this part of the loop.

The results are summarized in Table 10.6: The magnetization values of the three different cubes show a difference of up to 0.6% (Table 10.6). The value for the sphere exhibits the largest difference of 2% with respect to the average value of the cubes. (This may be a result of the grinding process in an air-pressure-driven mill. The sample is forced to rotate rapidly in a container of corundum.) It is possible that the surface structure of the sample may have been destroyed. If a disturbed surface layer of 40 µm is assumed, this could account for the deviation of the magnetization value.

Discussion of the Calibration Procedure

The field of a PFM is calibrated using a small pickup coil, where the effective winding area is known from NMR calibration. Using such a procedure allows an absolute field calibration of better than 1%, including the time constants (gain) of the integrator. The obtained field calibration also agrees within 2% with that of the PTB-calibrated magnet coercivity value.

In principle, nonconducting materials, such as Fe_3O_4 or a soft magnetic ferrite like 3C30, are better suited for this calibration. Unfortunately, the temperature dependence of the magnetization of the industrially available ferrite 3C30 is much worse then that of Fe_3O_4 (Fig. 10.40).

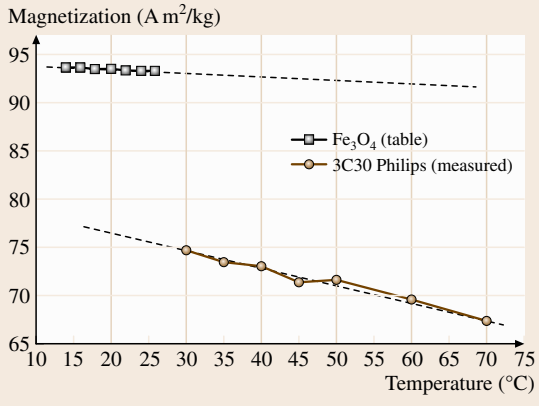

Fig. 10.40 Temperature dependence of the saturation magnetization of 3C30 compared with that of Fe_3O_4

The calibration constants using Fe_3O_4, Fe and Ni agree within 1.6%. The reproducibility of the different magnetization measurements – especially using Fe or Ni samples – was better than 0.3%. The error due to eddy currents in the rather long pulse duration (56 ms) is negligible. The zero signal of the system is less than 10% of the Fe_3O_4 sample signal, which has the smallest sample signal. According to these considerations, one can conclude that the sensitivity of the PFM investigated here is high enough to measure Nd-Fe-B magnet samples as small as 0.3 g mass, which corresponds to a cube of 3 mm × 3 mm × 3 mm. Such a PFM is, however, also capable of measuring samples with diameters up to 30 mm. It has to be mentioned that the sensitivity for a certain sample size depends mainly on the coupling between the sample and the pickup system. Therefore the sensitivity can be improved by adjusting the pickup system to a certain sample dimension.

If one works very carefully, an absolute magnetization calibration within ±1% is possible. Due to the good linearity of the analogue measuring electronics available nowadays and the high resolution of ADC cards (14 bit), a relative measurement – which is most important for a quality-control system – with a relative accuracy better than 0.5% is possible.

10.3.4 Hysteresis Measurements on Hard Magnetic Materials

Comparison Static Measurement – Dynamic Measurement

For testing a PFM system a set of commercial permanent-magnet samples was chosen: isotropic and anisotropic barium ferrite, anisotropic low- and high-coercivity Nd-Fe-B magnets. The shape of the samples was cylindrical: diameter 4 mm, length 5 mm; a demagnetizing factor of 0.255 was used. In order to allow a comparison between static hysteresis and dynamic hysteresis measurements a set of spheres (from the same batch of samples) were produced at the Technical University (TU) of Vienna.

In order to test the reliability of dynamic measurements pulsed field hysteresis loops where compared with static loops. In Fig. 10.41 the hysteresis loop as measured on an isotropic barium ferrite obtained in the static system at the Centre National de la Recherche Scientifique (CNRS) in Grenoble is compared with that

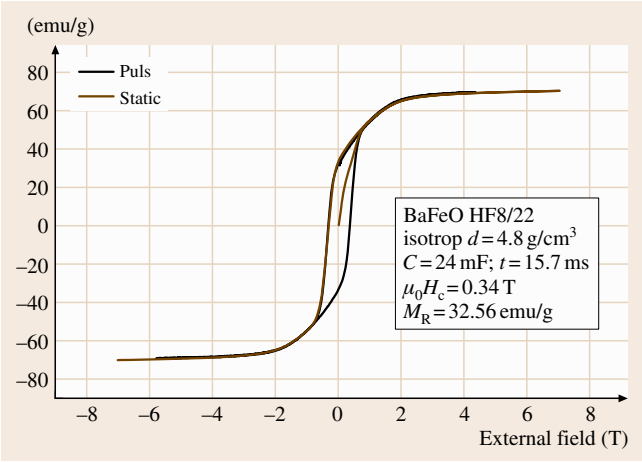

Fig. 10.41 Hysteresis loop as measured on the isotropic BaFeO HF 8/22 spherical sample

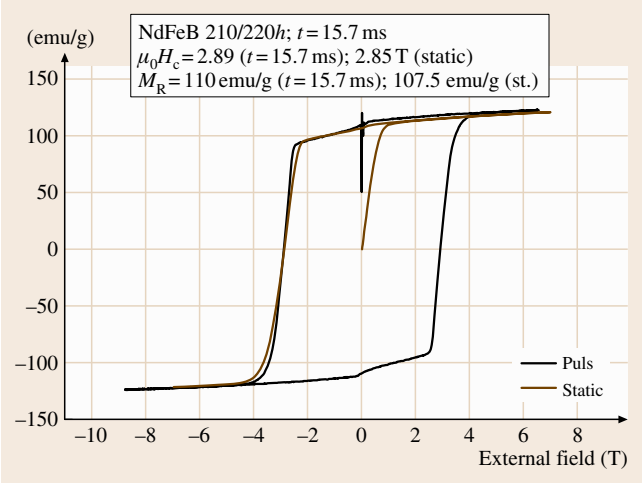

Fig. 10.42 Room-temperature hysteresis loop of a spherical Nd-FeB 210/220 magnet measured in a static magnetometer and in the pulsed field magnetometer

measured in the TU PFM. The use of barium ferrite has the advantage that there are no eddy currents because this material is an insulator. The difference is within the line thickness.

Figure 10.42 also shows for comparison hysteresis measurements on a Nd-Fe-B magnet as performed in the PFM (TU Vienna) and in the static magnetometer (CNRS Grenoble). There are differences in the slope of the $M(H)$ curve close to the coercivity. It is believed that this is due to small differences in the sphericity of the samples. This cannot be due to eddy currents in the sample because the coercivity value is the same. This shows that, for sample sizes below 10 mm, and for the pulse duration here used (15.7 ms) the eddy-current effects are negligible.

Rare-Earth-Based Magnets

For the following discussion of different types and shapes of rare-earth-based industrial magnets the room-temperature hysteresis loops were measured in the industrial PFM located at TU Vienna.

Figures 10.43 and 10.44 show such a loop as obtained from Vacodym 510 (a Nd-Fe-B magnet); the agreement between the static and pulsed data is very good. The applied field, especially in the second half wave, is not sufficient.

10.3.5 Anisotropy Measurement

Generally the magnetocrystalline anisotropy constants are determined from measurements on a single crystal in a torque magnetometer or similar device. Unfortunately single crystals are not available from many materials. In this case, polycrystalline material can sometimes be aligned in an external field and then the magnetization $M(H)$ is measured parallel and perpendicular to the external field. Curves determined in this way can be fitted, which also allows an estimate of the magnetocrystalline anisotropy to be made.

Another, sometimes better, possibility is to determine the magetocrystalline anisotropy field H_a using the so-called singular point detection (SPD) technique [10.44]. The principle of the SPD method is shown in Fig. 10.45. Single crystals are not necessary for the SPD method, and it allows the determination of the physically relevant anisotropy field even for polycrystalline samples. This is especially important when investigating technically relevant compositions, which often consist of many phases and exhibit rather complex compositions, such as e.g. $Sm(Co, Fe, Cu, Zr)_{7.5}$ which is typical for a so-called 2/17-based technical magnet [10.45]. Additionally many new technologies, such as rapidly quenching, hydrogenation disproportionation desorption recombination (HDDR), nitrogen loading or even thin films, lead to isotropic material, where single crystals are not possible in principal. In this case the SPD technique is the only possibility to determine the anisotropy field. Up to now this method was restricted to uniaxial systems. Recently it was extended to easy plane systems [10.46], which is essentially for many 3-D-dominated compounds.

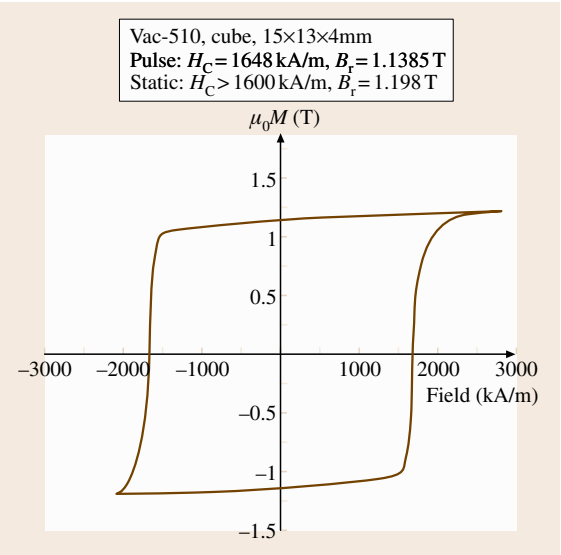

Fig. 10.43 Room-temperature hysteresis loop as obtained on a cube of Vacodym 510 (an Nd-Fe-B magnet)

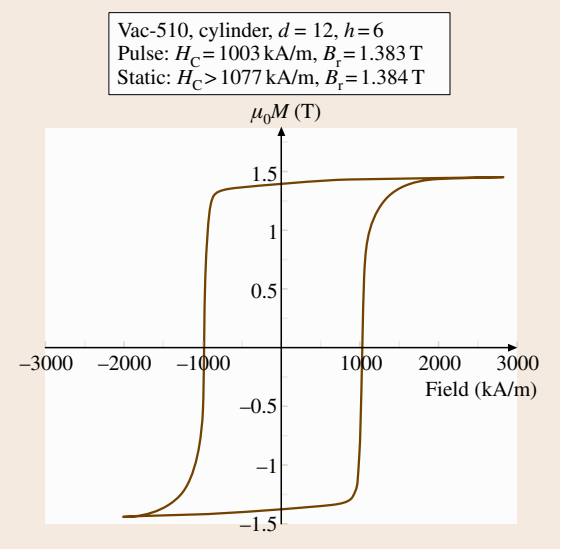

Fig. 10.44 Room-temperature hysteresis loop as obtained on a cylinder of Vacodym 510 (an Nd-Fe-B magnet)

Limitations of the SPD Method

The SPD method delivers only the anisotropy field H_a. This is technically relevant, but it is not sufficient for a deeper analysis based on the anisotropy constants. At least the anisotropy energy and its temperature dependence have to be known. If the real saturation magnetization can be determined the anisotropy energy

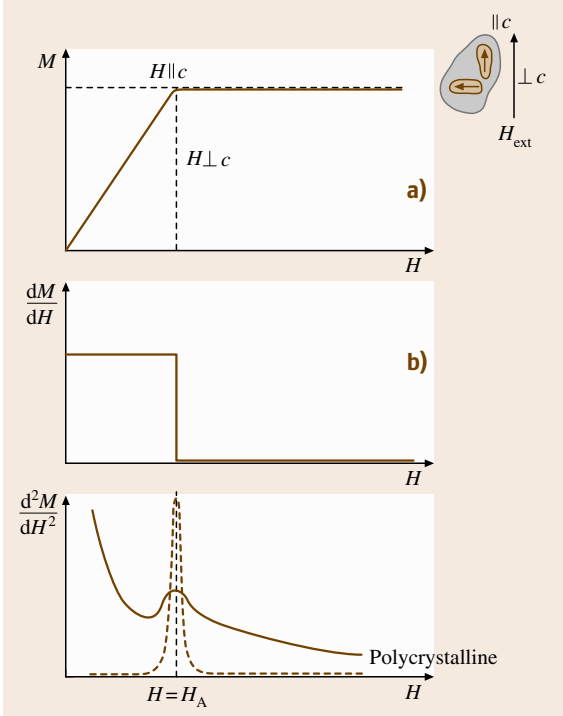

Fig. 10.45a–c The principle of the SPD measurement for determining the anisotropy field

can be calculated from H_a. Unfortunately an accurate determination of the saturation magnetization is not simple in hard magnetic compounds, because insufficiently high fields are available in usual magnetometers. For this purpose accurate magnetization measurements up to fields which are comparable to H_a (or larger) are necessary, and at different temperatures. When the temperature dependence of the anisotropy energy and that of the magnetization is known, various types of analysis such as scaling laws can be used in order to come to an understanding of these data. From such an analysis, information about the origin of the anisotropy can be deduced.

Studies performed in existing pulsed field systems (in Vienna and Parma) showed that the SPD method works well for anisotropy fields up to about 20 T. The reason for this limitation is that the maximum external field has to be at least 50% higher than H_a in order to make the singularity visible. Another limitation comes from the fact that at higher fields (above approximately 25 T) the vibrations and consequently the noise of the high-field system increases drastically, although this is not yet fully understood. Because the SPD method is

based on a differentiating technique ($d^2M(t)/dt^2$) the noise appearing at higher fields limits the measurable H_a values.

One of the basic problems here is that using a differentiating technique greatly increases all type of noise; and the high-frequency noise in particular increases with ω^2.

In the meantime the SPD method has been used to investigate the anisotropy field of many hard magnetic materials [10.47–49]. Some materials of interest recently where the measurement of the anisotropy field is only possible using the SPD method are the exchange coupled nanocrystalline hard magnetic materials.

The Anisotropy Field of Nanocrystalline Materials

It is not an easy task to determine the anisotropy field in these intrinsic isotropic samples. In addition, the strong magnetic exchange interaction among nanocrystallites makes measurements even more difficult. In this respect, singular point detection (SPD) provides a unique method for the direct determination of the anisotropy field of isotropic samples. In Fig. 10.46 the temperature dependencies of the anisotropy field measured for mechanically alloyed, nanocrystalline $Pr_9Fe_{85}B_6$, $Pr_{11.76}Fe_{82.36}B_{5.88}$ and $Pr_{18}Fe_{76}B_6$ is shown [10.50]. Here the sample $Pr_9Fe_{85}B_6$ represents a nanocomposite with $Pr_2Fe_{14}B$ and α-Fe; the $Pr_{11.76}Fe_{82.36}B_{5.88}$ should be single phase containing only $Pr_2Fe_{14}B$ grains whereas the $Pr_{18}Fe_{76}B_6$ should contain $Pr_2Fe_{14}B$ grains that are decoupled by an excess of Pr.

It is worth noting that the anisotropy field measured by using the SPD technique corresponds only to that of the hard magnetic phase. In the case of $Pr_9Fe_{85}B_6$ which consists of $Pr_2Fe_{14}B$ and α-Fe, that is the $Pr_2Fe_{14}B$ phase. The reduction of the anisotropy field in the nanocrystalline $Pr_{12}Fe_{14}B$ grains is a strong indication of the presence of magnetic exchange interactions. In the case of microcrystalline sintered Pr-Fe-B magnets the magnetic exchange interaction among the microsized grains is insignificant to influence the easy magnetization direction (EMD) of the grains. Thus the anisotropy field measured in the microcrystalline magnets corresponds to the anisotropy field of isolated $Pr_2Fe_{14}B$ grains. However, when the average grain size is reduced to nanometer size ($D_V < 50$ nm), the exchange interaction among the hard magnetic grains may become so strong that the EMDs of the nanocrystallites can be slightly tilted without the presence of external fields. The actual direction of the final EMD could be an energetic compromise of the surrounding nanocrystallites. This slightly tilted EMD gives a naturally reduction of the anisotropy field. This reduction of H_a also becomes visible in the SPD peak of the measurement of d^2M/dt^2 versus H, where the peak indicates the position of H_a (Fig. 10.47). From Fig. 10.46 a systematic decrease of H_a(T) with increasing coupling between the grains going from excess Pr content (18% Pr) to a stoichiometric sample (12% Pr) to a low-Pr-content material (9% Pr) becomes clearly visible for higher temperatures. For lower temperatures, because of the increasing anisotropy, a decoupling of the grains occurs that causes equal values of H_a for all three samples.

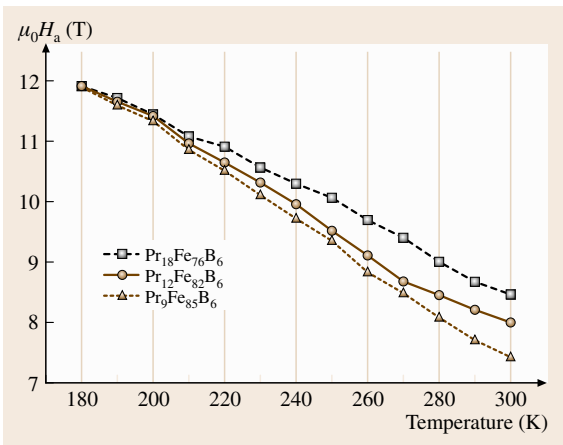

Fig. 10.46 The temperature dependence of the anisotropy field for hot-pressed mechanically alloyed Pr-Fe-B

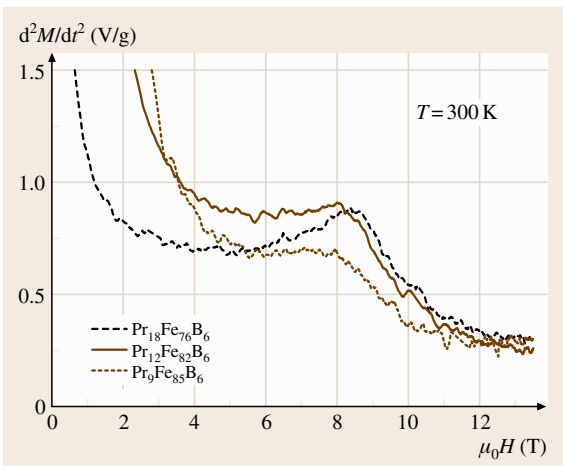

Fig. 10.47 The SPD peak measured at 300 K for mechanical alloyed hot-pressed Pr-Fe-B samples with nanosized grains

10.3.6 Summary: Advantages and Disadvantages of PFM

A PFM generally allows fast magnetization measurements in sufficiently high magnetic fields. Reproducible, nondestructive fields up to 40 T are nowadays the state of the art. Using a capacitor bank as an energy store allows the generation of a pulsed magnetic field in a volume that is best suited to solve a technical task. Therefore for many applications a PFM is much better suited than a standard static magnetometer, which is less flexible.

Comparison with static hysteresis loops demonstrated that, if both systems are calibrated careful, PFM measurements of hard magnetic materials are reliable and achieve a similar accuracy to that of a static system.

In terms of the demagnetizing field, correction for industrial shapes is not simple. For shapes like cylinders or cubes that are not too complex the use of a single factor is sufficient, but for other shapes this problem is still open. This is not only a problem for PFM, but occurs in all magnetic open circuits.

A general understanding of eddy currents now exists. The $f/2f$ method is a good fast method to correct for eddy-current errors in PFM measurements.

In principle magnetic viscosity causes an error in all hard magnetic materials. However, it seems that pinning-type materials exhibit a larger magnetic viscosity. The magnetic viscosity generally increases with the magnetocrystalline anisotropy. Therefore for room-temperature measurements on nucleation-type materials (ferrites, Nd-Fe-B, $SmCo_5$-based) this effect seems to be sufficient small.

To summarize, PFMs can be constructed that show better results then many static hysteresisgraphs however with the advantage that in a PFM higher fields are available, a faster measurement is possible and no special sample preparation is generally necessary. For ferrites and Nd-Fe-B-based magnets, fields up to 5 T are necessary, whereas for materials such as $SmCo_5$-based magnets, fields of approximately 10 T are necessary.

Beside the possibility of measuring a magnetization (hysteresis loop) a PFM can also be used to determine the anisotropy field using the SPD method, as was shown. This method is unique because it works even for polycrystalline materials.

10.4 Properties of Magnetic Thin Films

Magnetic thin films are receiving growing interest both from a fundamental scientific point of view and because of a variety of novel applications, in particular for magnetic-field sensors and information storage. Some of their specific properties relating to new technologies have already been mentioned in Sect. 10.1.5. In the present section the most important magnetic properties of magnetic thin films are discussed together with the most suitable methods of measuring the related quantities.

10.4.1 Saturation Magnetization, Spontaneous Magnetization

Phenomena

The saturation magnetization of a material M_{sat}, defined as the magnetic moment per volume, is of great technical interest because it determines the maximum magnetic flux that can be produced for a given cross section. However, M_{sat} as the *magnetization at technical saturation* is not a well-defined quantity because a large enough external magnetic field must be applied to produce a uniform magnetization by eliminating magnetic domains and aligning the magnetization along the field against magnetic anisotropies; however, at the same time the magnetization at any finite temperature $T > 0$ will continue to increase with increasing applied field (*high-field susceptibility*). The only well-defined quantity, hence, is the spontaneous magnetization M_S i. e. the uniform magnetization inside a magnetic domain in zero external field.

In practice, M_S is determined by measuring the magnetization as a function of the external field, $M(H)$ (which means the magnetization component parallel to the applied field) up to technical saturation, with a linear extrapolation of the data within the saturated region back to $H = 0$. A linear fit is a good approximation for temperatures well below the Curie temperature of the ferromagnetic material.

The method proposed above works best by applying the external field along an easy axis of magnetization and is especially well suited for thin films because of the absence of a demagnetizing field for in-plane magnetization; usually a relatively small field is sufficient

for saturation and the extrapolation to $H = 0$ is not required. Of course, higher fields are required for magnetically hard materials. In films having a dominating intrinsic anisotropy with a perpendicular easy axis the measurement should be done along the film normal.

When comparing the magnetization of a thin film to the value of the corresponding bulk material two different effects can be important.

1. The magnetization or the magnetic moment per atom in the ground state, i. e. at absolute zero temperature, might be enhanced. Depending on the specific combination of ferromagnetic material and substrate the enhancement may reach 30% for a single atomic layer (e.g. Fe on Ag or Au), but will disappear 3–4 atomic layers away from the interface. Depending on the band structure of the materials the magnetic moments at the interface may also be reduced in some cases (e.g. for Ni on Cu);
2. Thermal excitations which result in a decrease of M_S with increasing temperature are more pronounced in thin films compared to bulk material. In a film of 10 atomic layers of Fe on Au, M_S at room temperature is reduced by about 10% compared to bulk Fe. The origin of this effect is the reduced (magnetic) coordination at surfaces and interfaces, which leads to an enhanced excitation of spin waves; for the same reason the Curie temperature is reduced in ultrathin films compared to the bulk material.

Measurement Techniques and Instruments

A variety of methods are used to measure the magnetic properties of thin films. In many cases, especially for relatively thick films, the techniques used for bulk material can be applied as well (see the overview in Sect. 10.1.6). Here, the emphasis is put on the high sensitivity required for films thinner than about 100 nm and for ultrathin films with thicknesses down to 1 nm or less.

Magnetic moments m in terms of absolute values are determined with a suitable magnetometer from the field dependence of the moment, the so-called magnetization loop $m(H)$. The *magnetization* $M(H)$, i. e. magnetic moment per volume, is found by dividing the moment by the magnetic volume. For ultrathin films the main uncertainty on M often comes from the determination of the volume rather than from the magnetic moment itself.

Vibrating-Sample Magnetometer (VSM)

The vibrating-sample magnetometer (VSM) is probably the most widely used standard instrument. The principle of operation is described in Sect. 10.2 (Fig. 10.7). When the specimen oscillates between a set of pickup coils with a frequency of several 10 Hz to a few 100 Hz, the amplitude of the AC voltage induced in the pickup coils is proportional to the magnetic moment of the specimen and the vibration amplitude of the sample. The factor of proportionality depends on the entire geometry including the shape and size of the sample. This must be taken into account when an absolute calibration is carried out. The principle of measurement can be combined with an iron core electromagnet, or with air coils for low-field operation, or with a superconducting magnet for high-field applications. The VSM allows relatively fast measurements (1–10 min for a complete $M(H)$ loop, depending on the type of magnet and the required sensitivity), is flexible and easy to use. In particular, measurements at various angles can be made with the great precision required for the determination of magnetic anisotropies. The sensitivity attainable depends largely on the geometry and position of the pickup coils. Standard versions are useful for magnetic moments corresponding to Fe or NiFe films more than 5 nm thick (assuming a lateral size of 1–2 cm). Thinner films of 1 nm or less can be measured with an optimized VSM. The sensitivity is generally reduced for variable-temperature measurements when a cryostat or oven must be mounted.

The SQUID Magnetometer

The SQUID magnetometer is based on the same principle as the VSM but with a superconducting pickup coil circuit and a superconducting quantum interference device (SQUID) as the flux detector. The structure of a commercial SQUID magnetometer is schematically shown in Fig. 10.48 [10.51].

The sample executes a periodic linear motion with a vibration frequency of 0.1–5 Hz. This causes a change of magnetic flux in the pickup coils, which are part of the totally superconducting circuit outlined in Fig. 10.49.

The SQUID itself is operated in a constant-flux mode and serves as an extremely sensitive zero-detector in the feedback loop outlined in Fig. 10.49. The output signal of the magnetometer is proportional to the current in the feedback coil required to compensate the flux change sensed by the pickup coils.

The detection limit of the SQUID magnetometer for magnetic moments is about 1000 times lower than that of the VSM, i. e. about 10^{-9} Gcm^3 or 10^{-18} V s m. It is usually combined with a superconducting magnet

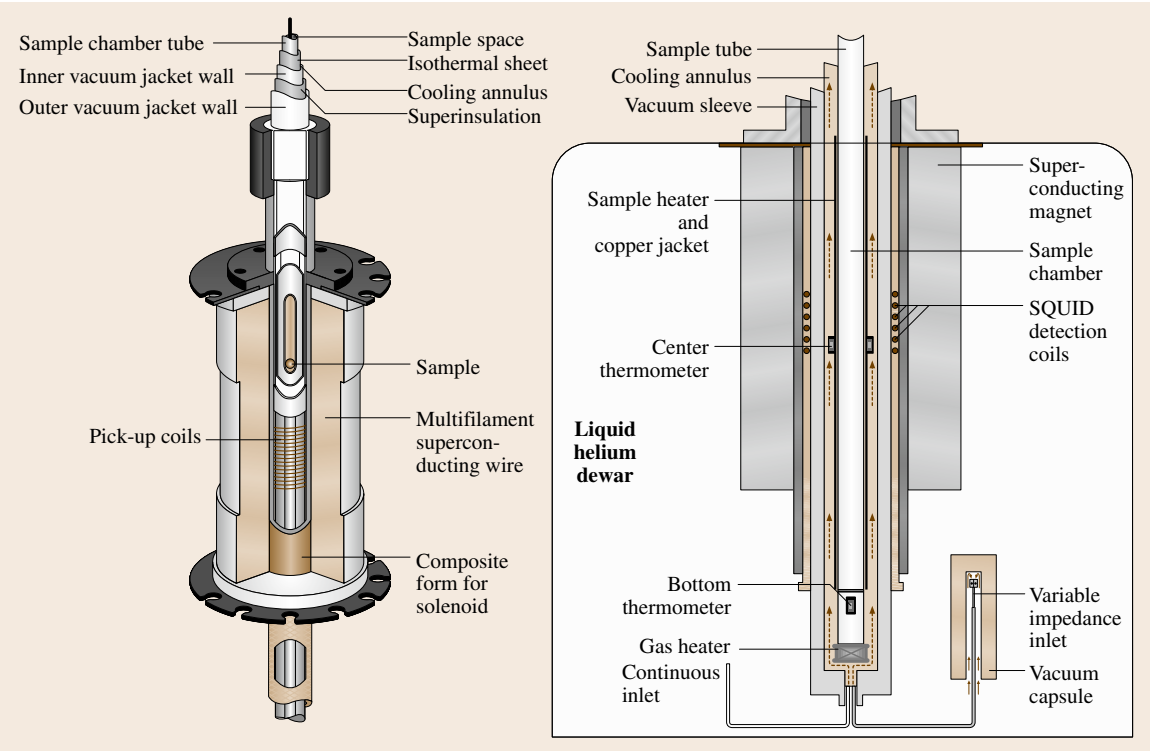

Fig. 10.48 Schematic view of a commercial SQUID magnetometer consisting of a liquid-He cryostat, a superconducting magnet, the variable-temperature sample chamber with thermometers and the detection coils close to the sample position. After [10.51]

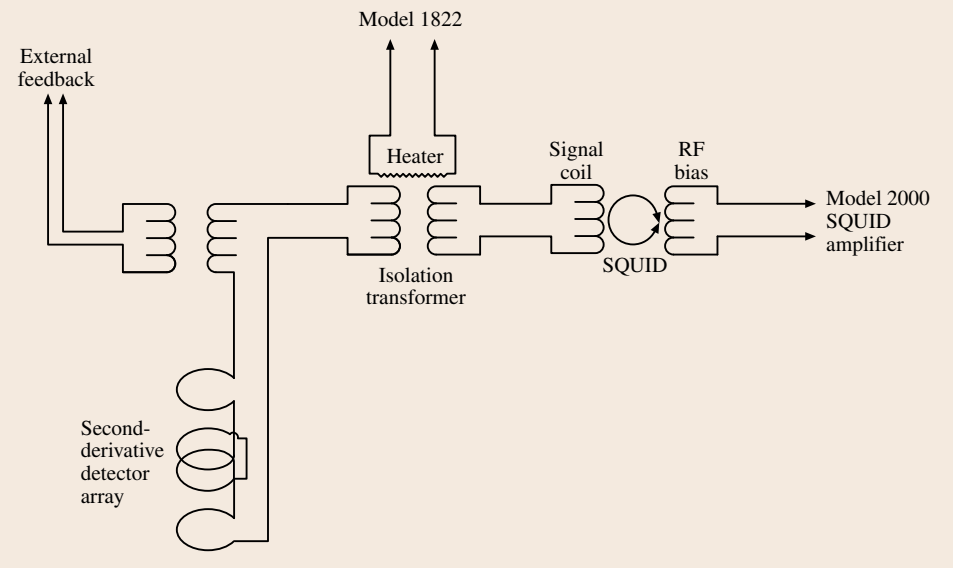

Fig. 10.49 Schematic diagram of the circuit of a commercial SQUID magnetometer (Quantum Design Inc.). All the coils are superconducting. The SQUID amplifier transforms any flux change sensed by the detector coils into a current, which is fed to the feedback coils such that this flux change is exactly compensated. This compensating current at the same time constitutes the output signal of the magnetometer. After [10.51]

and a variable-temperature He cryostat, which allows for measurements in high fields (3–7 T for commercial instruments) and at low temperatures. The biggest challenge is to make use of the high sensitivity of the SQUID in the presence of unavoidable fluctuations of the field from the external magnet. The most efficient solution is to use carefully balanced pickup coils in the form of a gradiometer of first or second order (e.g. a second-order gradiometer is shown in Fig. 10.49).

Typical measuring times for a complete magnetization loop may range from 30 min up to a full day depending on the field range and number of data points. For precision measurements a careful calibration that takes into account the specific sample geometry is necessary. For most purposes the SQUID magnetometer is the most suitable and versatile instrument for measuring extremely thin films in a wide range of temperatures (typically 2–400 K) and applied magnetic fields (up to 7–9 T).

The Alternating (Field) Gradient Magnetometer

The alternating (field) gradient magnetometer (AGM or AFGM) is a modification of the well-known Faraday balance that determines the magnetic moment of a sample by measuring the force exerted on a magnetic dipole by a magnetic field gradient. The principle of the instrument [10.52] is sketched in Fig. 10.50. The force is measured by mounting the sample on a piezoelectric bimorph, which creates a voltage proportional to the elastic deformation and, hence, to the force acting on the sample. By driving an alternating current through the gradient coils, with lock-in detection of the piezo voltage and by tuning the frequency of the field gradient to the mechanical resonance of the sample mounted on the piezoelectric element by a glass capillary a very high sensitivity can be achieved that approaches that of a SQUID magnetometer under favorable conditions. The main advantage of the AGM is its relative immunity to external magnetic noise and the resulting high signal-to-noise ratio and short measuring time. A major disadvantage is the difficulty in obtaining an absolute calibration of the magnetic moment because the signal is not only proportional to the sample magnetic moment but also to the Q-factor of the sample-capillary-piezo system, which varies with sample mass and temperature. This problem can be overcome by inserting a small calibration coil close to the sample position. Also, difficulty in obtaining an exact angular orientation of the sample relative to the external magnetic field is a drawback of this instrument. An AGM is relatively easy to build, but is also commercially available. It can be equipped with a cryostat or oven for variable-temperature measurements.

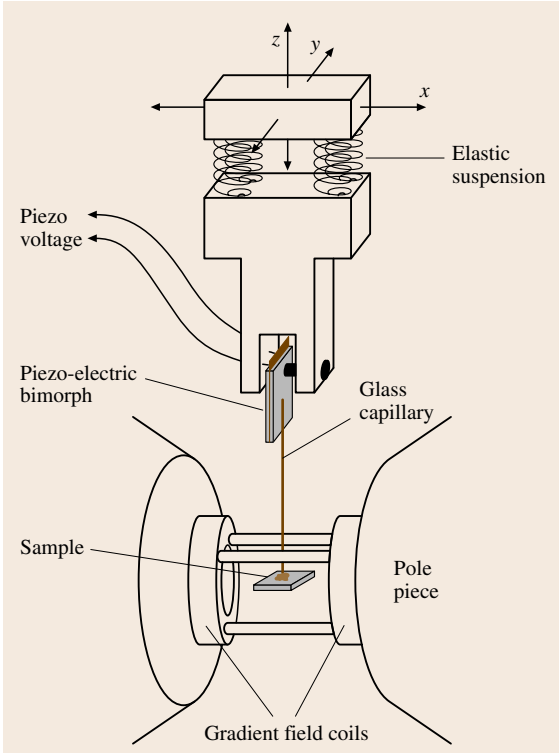

Fig. 10.50 Principle of the alternating (field) gradient magnetometer (AGM/AFGM); the gradient field coils are fed with an alternating current with a frequency tuned to the mechanical resonance of the sample-capillary-piezo system. The sample and gradient coils are mounted between the pole pieces of an electromagnet

Torque Magnetometers

Torque magnetometers in the form of a torsion pendulum (Sect. 10.2.2) have been successfully used for ultrathin films due to the high sensitivity attainable [10.53]. However, they measure the effective magnetic anisotropy of the sample; therefore, the different contributions to the anisotropy of the given sample must be known in order to determine the magnetic moment. This is further discussed in the next section.

Magnetooptic Techniques

When only the shape of the magnetization loop, or the relative variation of the magnetization with temperature, orientation of the external field or another external parameter is of interest, *magneto-optic effects*

(magneto-optic Faraday effect or Kerr effect, MOKE) are very useful. Because of the limited penetration depth of light magneto-optic techniques only probe the first 10–50 nm below the surface of a metallic sample and are therefore well suited for the fast characterization of magnetic thin films. For these, MOKE is a particularly powerful technique [10.54].

A typical arrangement is sketched in Fig. 10.51.

Upon reflection from a magnetic surface a beam of linearly polarized light in general will change its state of polarization depending on the relative orientation of the magnetization of the sample and the polarization axis. Both the ellipticity ε_K and Kerr rotation angle of the polarization δ_K occurring due to reflection can be used to measure a certain magnetization component defined by the specific arrangement. Basically, there are three different arrangements: i) the polar Kerr effect is measured with (nearly) perpendicular incidence of the light beam; the magnetizing field is applied perpendicular to the film plane and δ_K is proportional to the perpendicular component of the magnetization; ii) the longitudinal Kerr effect is observed with the light beam at oblique incidence and the in-plane magnetization component parallel to the plane of incidence is measured; iii) the transverse Kerr effect, which is observed in the same geometry as the longitudinal MOKE, produces a change of the intensity of the reflected beam and is proportional to the magnetization component perpendicular to the plane of incidence.

Gas lasers like He-Ne or laser diodes are equally used for MOKE measurements provided that the intensity and polarization are sufficiently stable. Various modulation techniques in combination with synchronous detection have been used to enhance the signal-to-noise ratio. A careful arrangement allows for very high sensitivity that is sufficient to measure the magnetization loops of films of less than a single atomic layer [10.55].

A major advantage of the MOKE technique is the possibility to focus the laser spot at the sample surface to less than 1 μm and thus measure magnetic properties with high lateral resolution. This is especially useful when the thickness dependence of properties is investigated by producing wedged samples with a lateral thickness variation. Another characteristic feature is the limited penetration depth of visible light of a few 10 nm in typical metal films; this allows measurements with a certain depth resolution, which is especially interesting for investigating multilayer structures. This can be further enhanced by choosing an appropriate wavelength for the light source according to the materials

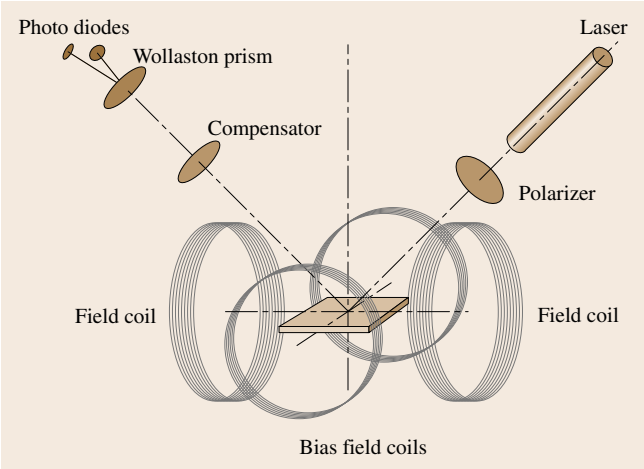

Fig. 10.51 Outline of a set up for magneto-optic Kerr-effect (MOKE) measurements (see text)

of interest, because the Kerr angle δ_K and Kerr ellipticity ε_K vary with the material and wavelength of the light.

MOKE, on the other hand, does not allow for a quantitative measurement of the absolute value of the magnetization. However, it is one of the most useful tools to investigate magnetic anisotropies, temperature dependence of magnetization and fast magnetization dynamics in magnetic films.

Magneto-optic effects in the (soft) x-ray energy range, in particular x-ray circular magnetic dichroism (XMCD), offer a unique potential: by tuning the photon energy to a core-level absorption edge it is possible to measure magnetic moments in an element-specific way. Furthermore, orbital and spin magnetic moments of electrons can be separately determined via so-called sum rules. This technique requires a synchrotron radiation source with circular polarization.

10.4.2 Magneto-Resistive Effects

Magneto-resistance means that the electric resistance of a material changes upon the application of a magnetic field. All conductive materials show magneto-resistive effects. However, here the discussion is restricted to magneto-resistance of ferromagnetic materials based on several different mechanisms.

Anisotropic Magneto-Resistance (AMR)

The dependence of the electric resistance on the angle θ between the magnetization and the current in a ferromagnetic material is called anisotropic magneto-

resistance (AMR) and can be described by

$$R(\theta) - R_0 = a\cos^2\theta \,. \tag{10.54}$$

The relative resistance change amounts to a fraction of a percent in most materials, up to 3% in permalloy films. The AMR effect has proved to be very useful for magnetic sensors.

Giant Magneto-Resistance (GMR)

The giant magneto-resistance effect is observed in layered magnetic film systems consisting of at least two ferromagnetic layers separated by a nonmagnetic metallic interlayer. When the magnetization in neighboring magnetic layers is switched from an antiparallel to a parallel configuration the electric resistance changes by an amount ranging from a few percent for two ferromagnetic layers to about 200% in special multilayer stacks. The GMR effect results from the spin-dependent scattering of electrons inside the layers and at the interfaces. For most materials the overall scattering rate is stronger for the antiparallel configuration, making it the high resistance state. In principle, the GMR can be observed both with the current flowing in the film plane (current-in-plane (CIP) configuration) or perpendicular (current-perpendicular-to-plane (CPP) configuration). However, measurement of the CPP-GMR due to the small junction resistance requires either the use of superconducting leads or restricted lateral junction dimensions of 100 nm or less.

An obvious application of GMR junctions is for magnetic-field sensors. The most suitable configuration is the so-called spin valve, which consists of a free magnetic layer that is easily magnetized along a small external field, a nonmagnetic metallic interlayer (Cu in most cases) and a hard magnetic layer with its magnetization pinned to a fixed direction by exchange coupling to an antiferromagnetic layer. The resistance R of such a device varies with the angle θ of the free layer magnetization as

$$R(\theta) - R_{\min} = c\cos\theta \,. \tag{10.55}$$

Compared to the characteristics of an AMR element it is obvious that GMR is more useful as an angle sensor, and this is indeed an attractive application of this effect. The most successful application, however, is still in read heads for hard-disc drives, where it has contributed to the steady increase in areal storage density.

Tunnel Magneto-Resistance

The tunnel magneto-resistance (TMR) is observed in ferromagnetic double-layer structures with an intermediate insulating layer. If the insulator is very thin, i. e. typically 1–2 nm, and a small voltage is applied between the two magnetic metallic contacts then a current will flow by a quantum-mechanical tunneling process. Similarly to the GMR effect the current depends on the relative orientation of the magnetization in both layers, with a large current flowing in the parallel configuration. The magnetization in one of the layers is frequently pinned by exchange coupling to an antiferromagnet (*exchange bias*) as in a spin-valve. As a consequence, the tunnel resistance varies with the angle of the magnetization of the free layer in the same way as for GMR as discussed above. Over the years the TMR ratio at room temperature in state-of-the-art magnetic tunnel junctions of FeCo layers and Al-oxide tunnel barriers has been increased to about 50% in moderate external fields, which makes them a very attractive field sensor. It should be noted, however, that the TMR ratio decreases strongly with increasing bias voltage and tunneling current. This has to be taken into account when different magnetic tunnel junctions (MTJs) are compared.

The most spectacular application of MTJs – besides hard disk read heads – is in all-solid-state fast magnetic random-access memories (MRAMs), which are now in an early state of production. A very promising recent achievement is a room-temperature TMR ratio of 500% and more obtained in junctions with a MgO tunnel barrier. This opens the way to an even brighter future for devices based on the TMR effect.

Colossal Magneto-Resistance

Extremely large magneto-resistance effects of more than 10 000% have been observed in certain compounds, especially in manganites with a perovskite structure. This effect is related to a metal–insulator transition which can be driven by a magnetic field. However, the largest effects are only observed at low temperatures and in very high fields, making these materials of limited technical value.

References

10.1 R. Grössinger, M. Taraba, A. Wimmer, J. Dudding, R. Cornelius, P. Knell, P. Bissel, B. Enzberg-Mahlke, W. Fernengel, J.C. Toussaint, D. Edwards: Calibration of an industrial pulsed field magnetometer, IEEE Trans. Magn. **38**(5), 2982–2984 (2002)

10.2 E.P. Wohlfarth: *Experimental Methods in Magnetism* (North-Holland, Amsterdam 1967)

10.3 E. Steingroever, G. Ross: *Magnetic Measuring Techniques* (Magnet-Physik Dr. Steingroever, Cologne 2009)

10.4 E. Steingroever: Some measurements of inhomogeneous permanent magnets by the pole-coil method, J. Appl. Phys. **37**, 1116–1117 (1966)

10.5 S. Foner: Versatile and sensitive vibrating-sample magnetometer, Rev. Sci. Instrum. **30**, 548–557 (1959)

10.6 R. Beranek, C. Heiden: A sensitive vibrating sample magnetometer, J. Magn. Magn. Mater. **41**, 247–249 (1984)

10.7 H. Zijlstra: Measurement of magnetic quantities. In: *Experimental Methods in Magnetism*, Vol. 2, ed. by E.P. Wohlfarth (North-Holland, Amsterdam 1967) pp. 168–203

10.8 S.R. Trout: Use of Helmholtz coils for magnetic measurements, IEEE Trans. Magn. **24**, 2108–2111 (1988)

10.9 B.D. Cullity: *Introduction to Magnetic Materials* (Addison-Wesley, Reading 1972) pp. 72–73

10.10 L.R. Moskowitz: *Permanent Magnet Design and Application Handbook* (Cahners Books International, Boston 1976) pp. 128–131

10.11 G. Bertotti, E. Ferrara, F. Fiorillo, M. Pasquale: Loss measurements on amorphous alloys under sinusoidal and distorted induction waveform using a digital feedback technique, J. Appl. Phys. **73**, 5375–5377 (1993)

10.12 D. Son, J.D. Sievert, Y. Cho: Core loss measurements including higher harmonics of magnetic induction in electrical steel, J. Magn. Magn. Mater. **160**, 65–67 (1996)

10.13 H. Ahlers, J.D. Sievert, Q. Qu: Comparison of a single strip tester and Epstein frame measurements, J. Magn. Magn. Mater. **26**, 176–178 (1982)

10.14 J. Sievert, H. Ahlers, P. Brosin, M. Cundeva, J. Luedke: Relationship of Epstein to SST. Results for grain-oriented steel, Proc. 9th ISEM Conf., Vol. 18, ed. by P. di Barba, A. Savini (IOS, Amsterdam 2000) pp. 3–6

10.15 H. Pfützner, P. Schönhuber: On the problem of the field detection for single sheet testers, IEEE Trans. Magn. **27**, 778–785 (1991)

10.16 E. Steingroever: A magnetic saturation measuring coil system, IEEE Trans. Magn. **14**, 572–573 (1978)

10.17 H. Ahlers: Polarization. In: *Units in Physics and Chemistry*, Landolt–Börnstein: Numerical Data and Functional Relationships in Science and Technology – New Series, Vol. Subvol. a, ed. by O. Madelung (Springer, Berlin, Heidelberg 1991) pp. 2–288–2–294

10.18 H. Wilde: Die Vorteile der Gegeninduktivitätsmeßbrücke bei ferromagnetischen Messungen, Int. J. Electron. Commun. (AEÜ) **6**, 354–357 (1952), (in German)

10.19 E. Blechschmidt: *Präzisionsmessungen von Kapazitäten, Induktivitäten und Zeitkonstanten* (Vieweg, Braunschweig 1956), (in German)

10.20 K.P. Koo, F. Bucholtz, A. Dandridge, A.B. Tveten: Stability of a fiber-optic magnetometer, IEEE Trans. Magn. **22**, 141–143 (1986)

10.21 IEC/TR 62581: Electrical steel – Methods of measurement of the magnetostriction characteristics by means of single sheet and Epstein test specimens (IEC, 2010)

10.22 R. Becker, M. Kersten: Die Magnetisierung von Nickeldraht unter starkem Zug, Z. Phys. **64**, 660 (1930), (in German)

10.23 K. Narita, J. Yamasaki, H. Fukunaga: Measurement of saturation magnetostriction of a thin amorphous ribbon by means of small-angle magnetization rotation, IEEE Trans. Magn. **16**, 435–439 (1980)

10.24 R. Grössinger, G. Herzer, J. Kerschhagl, H. Sassik, H. Spindler: An. Fis. B **86**, 85–89 (1990)

10.25 C. Polak, R. Grössinger, G. Vlasak, L. Kraus: J. Appl. Electromagn. Mater. **5**, 9–17 (1994)

10.26 K. Mohri, T. Kohzawa, K. Kawashima, H. Yoshida, L.V. Panina: IEEE Trans. Magn. **28**(5), 3150–3152 (1992)

10.27 R.S. Beach, A.E. Berkowitz: Appl. Phys. Lett. **64**(26), 3652–3654 (1994)

10.28 F.L.A. Machado, C.S. Martins, S. Rezende: J. Phys. Rev. B **51**(6), 3926–3929 (1995)

10.29 M. Knobel, M.L. Sartorelli, J.P. Sinnecker: Phys. Rev. B **55**, R3362–R2265 (1997)

10.30 R. Grössinger, X.C. Kou, M. Katter: Physica B **177**, 219–222 (1992)

10.31 R. Grössinger, M. Taraba, A. Wimmer, J. Dudding, R. Cornelius, P. Knell, B. Enzberg-Mahlke, W. Fernengel, J.C. Toussaint: Proc. 17th Int. Workshop Rare-Earth Magn. Appl. (Newark 2002) pp. 18–22

10.32 R. Gersdorf, F.A. Müller, L.W. Roeland: Colloq. Int. CNRS No. 166 (1967)

10.33 D. Eckert, R. Grössinger, M. Doerr, F. Fischer, A. Handstein, D. Hinz, H. Siegel, P. Verges, K.-H. Müller: Physica B **294/295**, 705–708 (2001)

10.34 R. Grössinger, M. Küpferling, P. Kasperkovitz, A. Wimmer, M. Taraba, W. Scholz, J. Dudding, P. Lethuillier, J.C. Toussaint, B. Enzberg-Mahlke, W. Fernengel, G. Reyne: J. Magn. Magn. Mater. **242–245**, 911–914 (2002)

10.35 D. Meecker: *Finite Element Method Magnetics* (Foster-Miller, Waltham 2004), http://femm.berlios.de/

10.36 M. Küpferling: Diploma Thesis (TU Vienna, Vienna 2001)

10.37 G.W. Jewell, D. Howe, C. Schotzko: IEEE Trans. Magn. **28**, 3114–3116 (1992)

10.38 R. Grössinger, G.W. Jewell, J. Dudding, D. Howe: IEEE Trans. Magn. **29**, 29080–29082 (1993)

10.39 C. Golovanov, G. Reyne, G. Meunier, R. Grössinger, J. Dudding: IEEE Trans. Magn. **36**(4), 1222–1225 (2000)

10.40 D. Givord, M.F. Rossignol, V. Villas-Boas, F. Cebollada, J.M. Gonzales: In: *Rare Earth Transition Metal Alloys*, ed. by F.P. Missel (World Scientific, Sao Paulo 1996)

10.41 R. Street, R.K. Day, J.B. Dunlop: J. Magn. Magn. Mater. **69**, 106 (1987)

10.42 D. Givord, P. Tenaud, T. Vadieu: IEEE Trans. Magn. **24**, 19 (1988)

10.43 J.C. Téllez-Blanco, R. Sato Turtelli, R. Grössinger, E. Estévez-Rams, J. Fidler: J. Appl. Phys. **86**, 5157 (1999)

10.44 G. Asti: J. Appl. Phys. **45**, 3600 (1974)

10.45 X.C. Kou, E.H.C.P. Sinnecker, R. Grössinger, P.A.P. Wendhausen: IEEE Trans. Magn. **31**(6), 3638–3640 (1995)

10.46 X.C. Kou, E.H.C.P. Sinnecker: J. Magn. Magn. Mater. **157/158**, 83–84 (1996)

10.47 R. Grössinger, R. Krewenka, H. Kirchmayr, S. Sinnema, F.M. Yang, Y.K. Huang, F.R. de Boer: J. Less Common Met. **132**, 265 (1987)

10.48 R. Grössinger, X.C. Kou, T.H. Jacobs: J. Appl. Phys. **69**(8), 5596–5598 (1991)

10.49 J.C. Tellez-Blanco, X.C. Kou, R. Grössinger, E. Estevez-Rams, J. Fidler, B.M. Ma: Proc. 14th Int. Workshop Rare-Earth Magn. Appl., ed. by F.P. Missel, V. Villas-Boas, H.R. Rechenberg, F.J.G. Landgraf (World Scientific, Sao Paulo 1996) pp. 707–716

10.50 M. Dahlgren, X.C. Kou, R. Grössinger, J. Wecker: Proc. 9th Int. Symp. Magn. Anisotropy Coerc., ed. by F.P. Missel, V. Villas-Boas, H.R. Rechenberg, F.J.G. Landgraf (World Scientific, Sao Paulo 1996) pp. 307–316

10.51 Quantum Design, San Diego 1996

10.52 P.J. Flanders: J. Appl. Phys. **63**, 3940 (1988)

10.53 U. Gradmann, W. Kümmerle, R. Tham: Appl. Phys. **10**, 219 (1976)

10.54 J.F. Dillon Jr.: In: *Magnetic Properties of Materials*, ed. by J. Smit (McGraw–Hill, New York 1971) p. 149

10.55 S.D. Bader, E.R. Moog, P. Grünberg: J. Magn. Magn. Mater. **53**, L295 (1986)